XMM

XMM-Newton SAS scientific validation - SAS V5.1

XMM-SOC-USR-TN-0004 Issue 1.0

C.Gabriel[1], M.Guainazzi[1], M.Denby[2], J.Osborne[2], A.Talavera[1]

August 31, 2001

1) XMM-Newton Science Operation Center, VILSPA, ESA, Apartado 50727, E-28080 Madrid, Spain

2) XMM-Newton Science Survey Center, Department of Physics & Astronomy, University of Leicester, Leicester LE1 7RH, UK

.

Contents

1 Introduction

The scientific validation aims at ensuring a constant high quality of the XMM-Newton Science Analysis System (SAS). It is in principle based on the results of the analysis of a number of specific observations, both through the SAS Pipeline System (PPS) as well as interactively. It aims to establish:

- which instrumental modes are fully supported by SAS,
- which scientific products can be produced by SAS, and
- the level of accuracy associated with those products.

Details of the Scientific Validation Plan, as well as the reference dataset chosen, are given in Gabriel et al (2000). In the run corresponding to SAS V5.1 we had 9 datasets available for testing, out of the basic 18 listed in that document.

In the following, we will list the data which had to be processed by the PPS, dataset by dataset, including the results of the default screening as applied to all XMM-Newton data after pipeline processing. The process failures will be listed with the corresponding explanations. The results of the special interactive analysis performed on some of the datasets for investigation of certain aspects of SAS analysis / calibration are presented and discussed in the following sections.

The list of calibration files used by the analysis is given in Appendix A of this document, the corresponding release notes are under http://xmm.vilspa.esa.es/ccf/releasenotes.

2 Input data

The 9 datasets tested during SV are listed in Table 2.

Data set	MOS	pn	RGS	OM	Comments
AB Doradus	—	Small Window	HER+SES	—	Processed
BPM16274	—-	—–	HER+SES	IMG+Grism	Processed
Capella	Full window	—	HER+SES	—	Processed
Crab Nebula	Part RFS	—	HER+SES	—	NOT Processed
EXO0748-676	Full window Partial W2	Full Frame Small window Large window	HER+SES	—-	Processed
G21.5-09	Full window	Full Frame	HER+SES	—	Processed
Lockman Hole	Full window	Full Frame	HER+SES	IMG	NO MOS2
Mrk 421	Fast Uncompressed Partial W4	Fast Timing	HER+SES	—	Processed
PKS0558-504	Full window Partial W3	Full Frame Small window	HER+SES HER+SES	IMG IMG	Processed

Table 1: SV test cases

3 Pipeline processing results

With the exception of one dataset, the Crab Nebula, all the SV data could be processed to completion. One MOS2 exposure (Lockman Hole) was not processed due to the camera temperature being below limits.

3.1 Not processed datasets

The Crab Nebula data failed in the processing because of a bug in the task *rgsfilter*. In this particular observation the RGS 2 exposure has no time interval during which all CCDs are giving good data simultaneously. This results in no good time interval for the data, and this is wrongly handled by the S/W, ending in an error. This problem, which could affect only a very low number of exposures, has been fixed but the fixed task is not yet part of the SAS 5.1., but will be in SAS 5.2.

3.2 Processed datasets

The PPS screening reports for each of the processed datasets, in

```
verbatim format
```

are presented here. These screening reports are produced by the SSC to highlight any anomalies in the pipeline processing, as first quality checks by every processed dataset. Therefore they should not be understood as a deep analysis of the results of each observation. To make them more comprehensive we have included some information as well as some illustrative figures.

3.2.1 AB Doradus:

XMM-Newton observed AB Doradus ($\alpha_{2000} = 5^h28^m44^s.0$, $\delta_{2000} = -65°27'02'.0$) , the nearest K-type Zero-Age-Main-Sequence (ZAMS) star, several times as routine calibration target. The observation used in this report took place on April 30, 2000, revolution 72, lasting more than 62000 seconds. Güdel et al. (2001) have published results partly based on this observation.

```
XMM SSC data-product screening log
Version: <23-05-2001>

XMM  XMM                 PCMS
Rev  Obs Seq.    Target  Seq_id
072  0123720201  AB Dor  000193


** GENERAL COMMENTS

No MOS and OM products. MOS CalClosed.
OM listed as inactive in observation summary, no OM ODF observation files.
2 exposures from RGS1 and RGS2.
Long duration PN and 1st RGS exposures, shorter duration 2nd RGS exposures.
Link to non-existent catalogue summary in observation summary page.
```

```
[EPIC comments refer, in general, to Energy-band 8.]

** EPIC MOS1

No products, CalClosed.


** EPIC MOS2

As MOS1.


** EPIC PN

Small window. Bright source on one side producing out of time events.
No source lists and exposure sensitivity map.


** RGS1, RGS2

2 exposures from RGS1 and RGS2, durations of 50000 and 12100 seconds.
All CCDs working in RGS1.

1st RGS1: Spatial extraction region place slightly too low on spatial map.
Clear bright spectrum slightly outside of spatial extraction region.
Clear bright spectra within spectral extraction regions on energy map.
Also third order spectrum just visible on energy map.
Clear spectra in the spectrum plots.

2nd RGS1: All spectra are fainter but still clear.
The spectrum plots are noisier, otherwise as 1st RGS1.

1st RGS2 as 1st RGS1, and 2nd RGS2 as 2nd RGS1.


** OM

No products, listed as inactive in observation summary.
No ODF observation files.


** Catalogue cross-correlation products

No products.
```

The main products of this observation are considered satisfactory. The PPS produced PN image in small window mode is given in Fig.1, while the RGS1 spatial and order image is shown in Fig.2 and the RGS1 extracted first and second order spectra are shown in Fig.3

The slightly off-centered RGS extraction region is due to the lack of source lists from the EPIC processing, MOS 1 & 2 did not view the sky, while PN small window mode exposures do not undergo source searching.

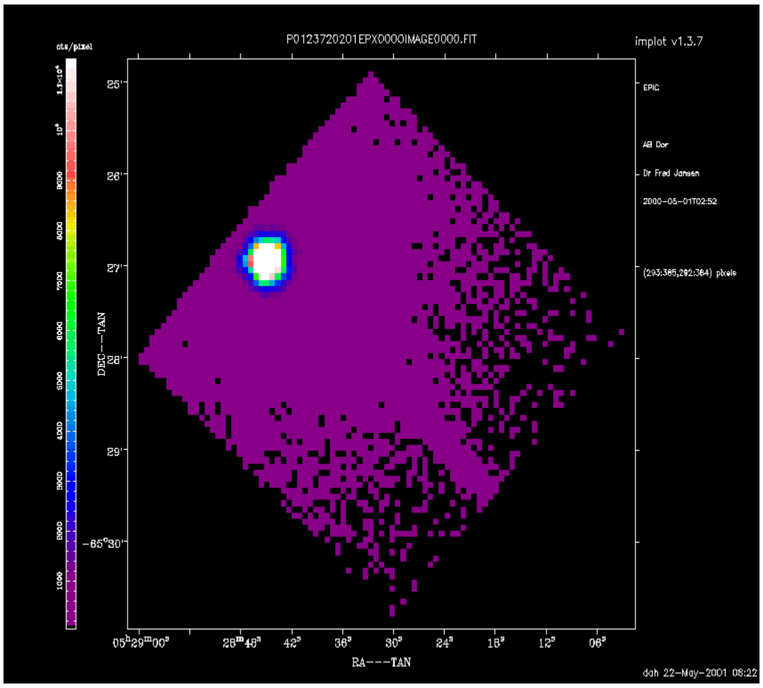

Figure 1: AB Doradus PN image, taken in PN small window mode

Results of interactive analysis on these data are given in section 4.3.

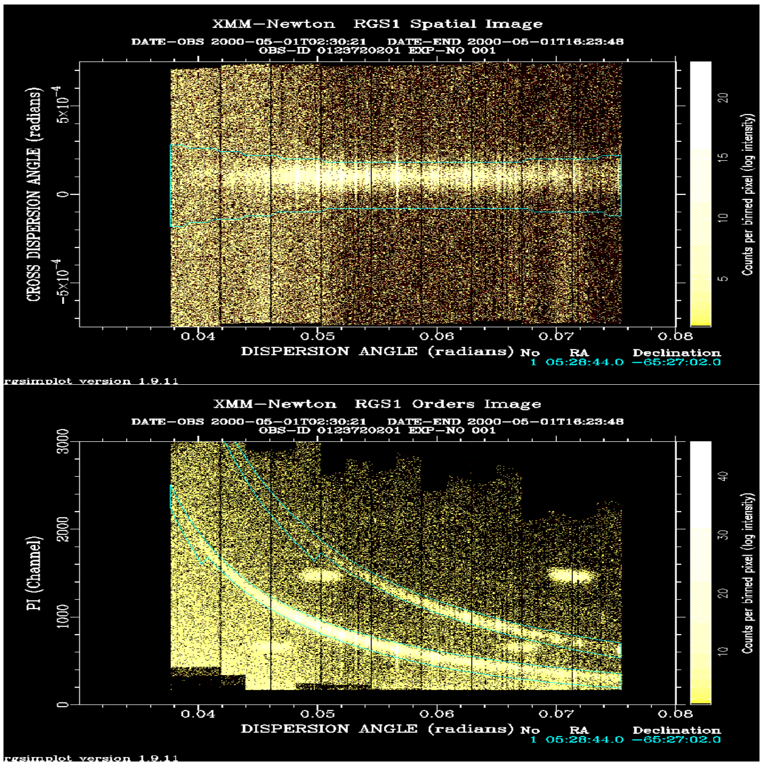

Figure 2: AB Doradus RGS1 spatial and orders images

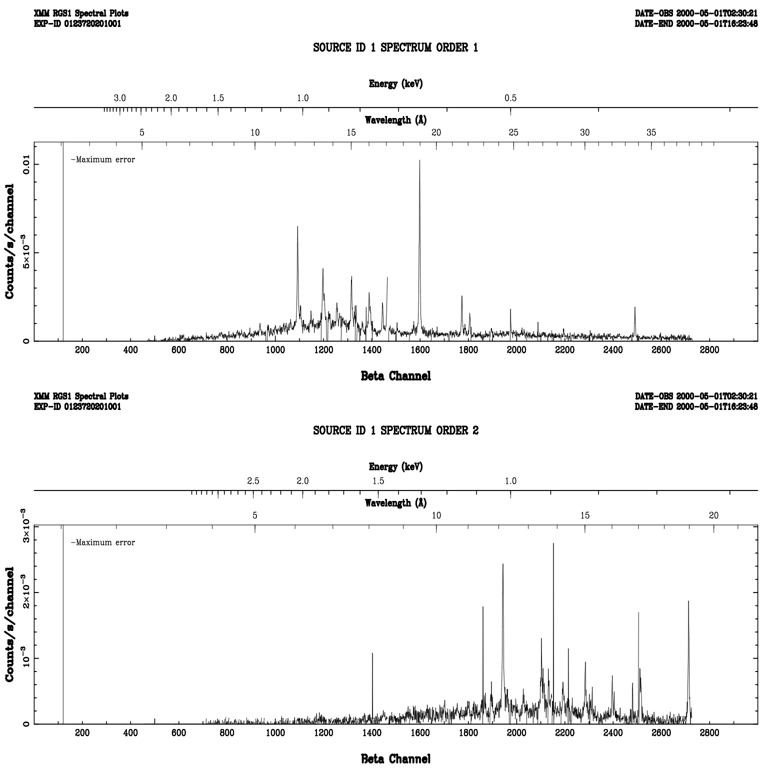

Figure 3: AB Doradus RGS1 first and second order spectra, as produced by PPS

3.2.2 BPM 16274

The White Dwarf BPM 16274 ($\alpha_{2000} = 0^h50^m3^s.18$, $\delta_{2000} = -52°08'17'.40$) is an OM calibration target. The observation used for SV was taken during revolution 81, containing 30 imaging exposures in 6 filters and a set of V grism exposures.

```
XMM SSC data-product screening log
Version: <18-07-2001>

XMM  XMM                  PCMS
Rev  Obs Seq.    Target    Seq_id
081  0123920101  BPM 16274  extra


** GENERAL COMMENTS

No MOS and PN products. MOS1 CalClosed, MOS2 Closed, PN Calibration Position.
(MOS and PN exposures extended because of high radiation levels).
6 sets of OM exposures using 6 filters.
No OM products from a further set of exposures taken with Grism2 over OM.
2 exposures from RGS1 and RGS2, long duration 2nd exposures.
Link to non-existent catalogue summary in observation summary page.


[EPIC comments refer, in general, to Energy-band 8.]

** EPIC MOS1

No products, CalClosed. (Exposure extended because of high radiation levels).


** EPIC MOS2

No products, Closed. (Exposure extended because of high radiation levels).


** EPIC PN

No products, PN filter was in Calibration Position.
(Exposure extended because of high radiation levels).


** RGS1, RGS2

2 exposures from RGS1 and RGS2, durations of 14320 and 43110 seconds.
All CCDs working in RGS1. Single blank column in 9th CCD of RGS2.
(2nd RGS1 exposure stopped because of a TC loss, some Q-Dumps lost).

Spatial extraction region to one side on spatial map.
Bright background and no spectra visible on spatial map and energy map.
Very noisy spectra in the spectrum plots.
```

```
2nd RGS1, 1st RGS2 and 2nd RGS2 all as 1st RGS1.


** OM

6 sets of exposures using the V, U, B, UVW1, UVM2 and UVW2 filters.
Exposure durations of 1000, 1000, 1000, 1160, 1320 and 1100 seconds.
Only sets 1-4 have tracking plots.
Links to non-existent tracking plots in the OM summary.
Tracking plot for exposure S496 shows 1 point 3 pixels from others.
Central diffuse object plus a long diffuse object and some other sources.

V & B  filters: Central ghost, loops (1 bright), 2 faint long parallel lines.
The bright loop is over the central diffuse object.
Bright sources are over-exposed, 2 have their own loops.
Small dark area in exposures S485 and S493.
The diffuse objects and a few sources not detected in the source lists.
A few spurious sources - bright extended objects, loops and background noise.

U filter: Faint central ghost, 1 bright loop and 1 faint long parallel line.
The bright loop is over the central diffuse object.
Bright sources are over-exposed, 2 have their own loops.
Small dark area in exposure S489.
The diffuse objects and a few sources not detected in the source lists.
A few spurious sources due to a loop and background noise.

UVW1 filter: 1 loop and 1 very faint long parallel line.
The loop is over the central diffuse object.
Bright sources are over-exposed, 1 has its own loop.
The central diffuse object and a few sources not detected in the source lists.
The long diffuse object is fainter but is now detected.
A few spurious sources due to a loop and background noise.

UVM2 filter: Only a few sources visible, long diffuse object not visible.
Central diffuse object not detected in the source lists.
A few spurious sources due to background noise.

UVW2 filter: Only a few sources visible, long diffuse object not visible.
Source lists OK, central diffuse object detected.


** Catalogue cross-correlation products

No products.
```

It has to be remarked that the main deficiencies in the OM processing are given by the lack of processing of the grism exposures, as well as the non detection of bright stars (including the target itself, due to high background features), except in the UV filters where there is almost no straylight. For the V, B, U filters, the target is about 100 times brighter than the straylight background. However, very faint stars with less than twice the background level are detected. The criteria used for detection should be revised. Figure 4 illustrates this.

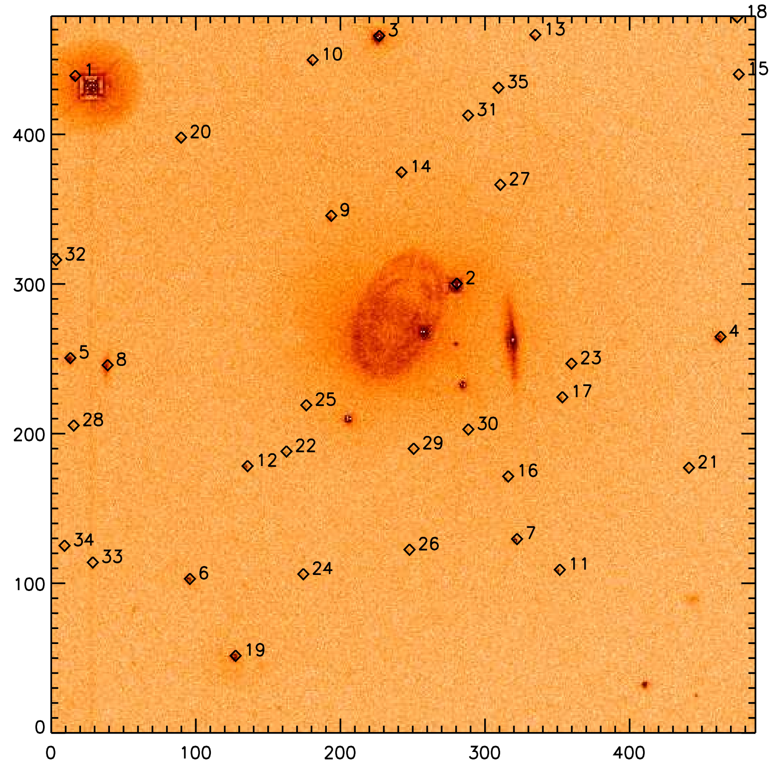

Figure 4: BPM 16274 OM image, V filter, with the positions of the found sources overlaid.

The astrometry of the found sources is satisfactory, the positions are within 2" from the catalogue positions.

There are still many deficiencies in the OM processing, despite many of the individual products are satisfactory and can be used for scientific analysis. The user is therefore urged to carefully apply her/his scientific judgment while analyzing the OM Data products.

3.2.3 Capella:

The binary star Capella ($\alpha_{2000} = 5^h16^m41^s.38$, $\delta_{2000} = 45°59'52'.80$), one of the brightest X-ray objects visible in the sky, is one of the main calibration targets of the XMM RGS instruments. High-resolution X-ray spectroscopy results have been published by Audard et al (2001) using the same data we use here for validation, a 55 ksec observation taken during revolution 54 on March 25, 2000.

```
XMM SSC data-product screening log
Version: <23-05-2001>

XMM  XMM                   PCMS
Rev  Obs Seq.    Target    Seq_id
054  0121920101  Capella   000187


** GENERAL COMMENTS

No MOS2, PN and OM products. MOS2 and PN modes undefined, OM blocked.
MOS1 exposure was unscheduled. Long duration RGS exposures, longer than MOS1.


[EPIC comments refer, in general, to Energy-band 8.]

** EPIC MOS1

Full frame. Bright central object, the centre of the object is blank.
Large cross of faint lines produced by the central object.
A few other sources in the field of view. Faint noisy columns.
All source lists affected by bright extended object.
Also spurious local sources due to the faint lines and background noise.
Many spurious map sources - the faint lines, field edge and background noise.


** EPIC MOS2

No products, mode was undefined.


** EPIC PN

No products, mode was undefined.


** RGS1, RGS2

All CCDs working in RGS1.

RGS1: Spatial extraction region placed correctly on spatial map.
Clear bright spectrum within spatial extraction region.
Clear bright spectra within spectral extraction regions on energy map.
Also third order spectrum visible on energy map.
```

```
Clear spectra in the spectrum plots.

RGS2: as RGS1.


** OM

No products, blocked.


** Catalogue cross-correlation products

A few XMM sources not already in the catalogue.
```

The main products of this observation are considered satisfactory. The PPS produced MOS1 image is strongly piled up, as expected, and shown in in Fig.5.

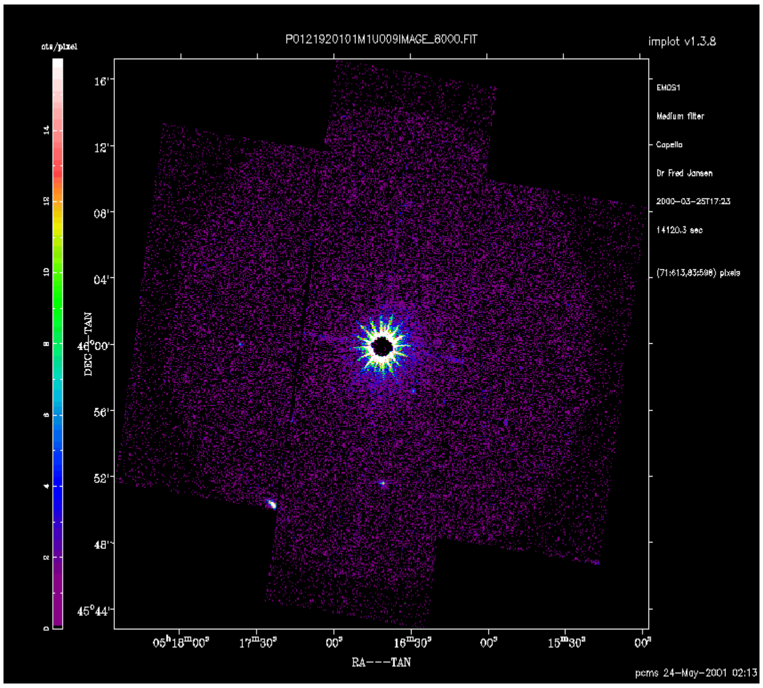

Figure 5: Capella image, taken in MOS 1 Prime Full Window mode

RGS1 spatial and order image is shown in Fig.6 and the RGS1 extracted first and second order spectra are shown in Fig.7. As specified in 4.3, they correspond to a pointing direction different from that originally entered in the proposal, the latter being wrong.

Results of interactive analysis on this data are given in section 4.3.

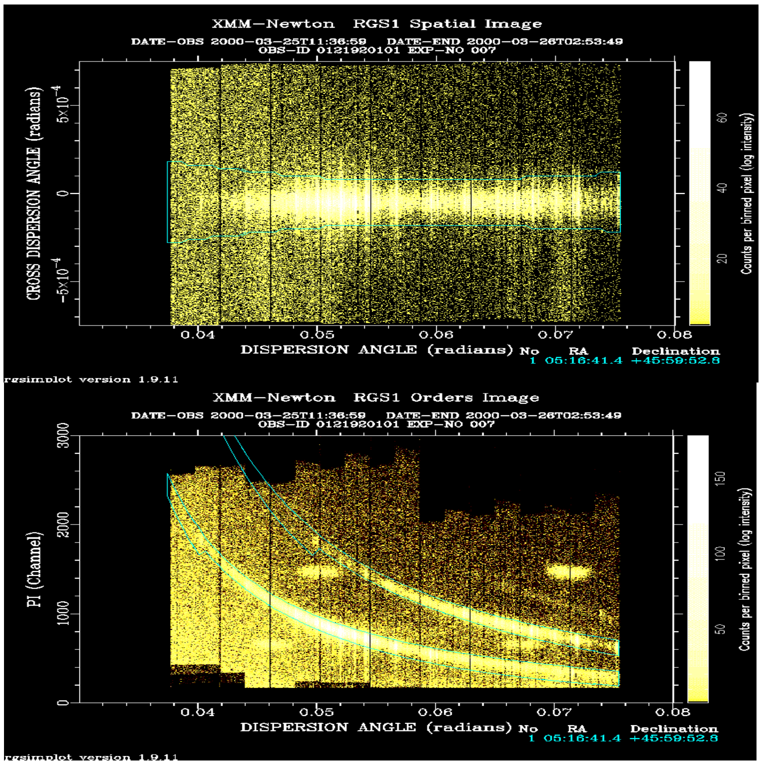

Figure 6: Capella RGS1 spatial and orders images

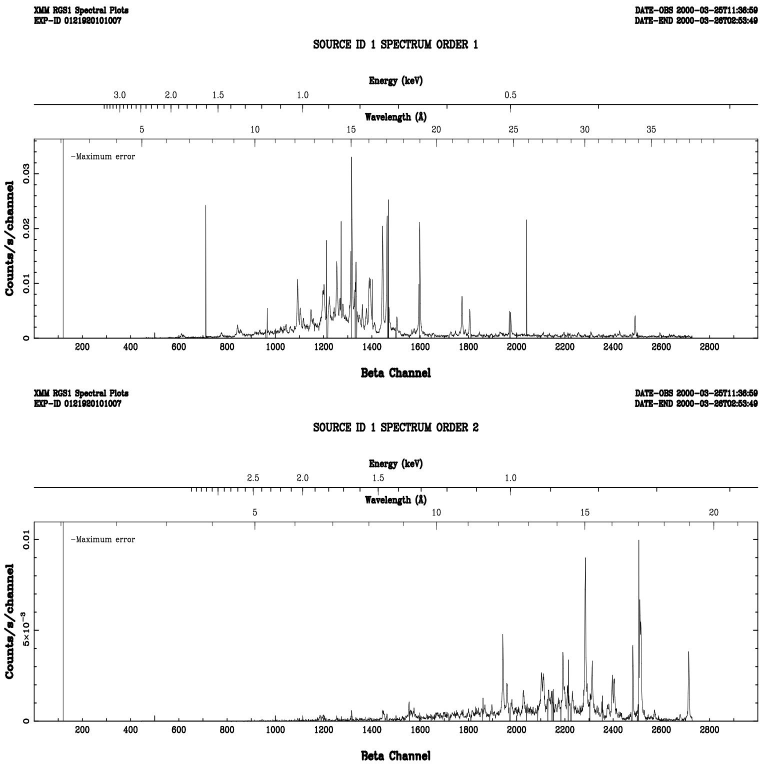

Figure 7: Capella RGS1 first and second order spectra, as produced by PPS

3.2.4 EXO0748-676:

The low mass X-ray binary EXO 0748-676 ($\alpha_{2000} = 07^h48^m24^s.50$, $\delta_{2000} = -67°45'0".00$), discovered with EXOSAT, has been observed by XMM-Newton during the Cal-PV phase several times, with published results with the EPIC cameras by Bonnet-Bidaut, et al (2001) and with the RGS spectrometers by Cottam et al (2001). We report here using the results of one 62 ksec observation, during which several exposures were taken with the EPIC MOS cameras in Full Window mode and Partial Window mode W2 (Small Window) and the EPIC PN camera in Full Frame mode, Large Window mode and Small Window mode, as well as with the RGS in the default (HER with SES) mode.

```
XMM SSC data-product screening log
Version: <29-05-2001>

XMM  XMM                 PCMS
Rev  Obs Seq.    Target    Seq_id
067  0123500101  EXO0748-676  000208


** GENERAL COMMENTS

No OM products, OM listed as inactive in observation summary.
No OM ODF observation files.
2 exposures from MOS1, MOS2, RGS1 and RGS2, 3 exposures from PN.
MOS and PN have shorter exposure durations than RGS.


[EPIC comments refer, in general, to Energy-band 8.]

** EPIC MOS1

Full frame and small window exposures, durations of 16798 and 2829 seconds.
Bright object just off-centre plus some other faint sources in the field.
All source lists affected by bright extended object.

Full frame: Large faint cross through middle of field. Faint noisy columns.
Spurious local sources due to background noise.
Many spurious map sources due to noisy columns, field edge, background noise.

Small window: Some spurious map sources due to field edge, background noise.


** EPIC MOS2

Full frame and small window exposures, durations of 16800 and 2862 seconds.
Bright object just off-centre plus some other faint sources in the field.
All source lists affected by bright extended object.

Full frame: A long faint line through middle of field. Faint noisy columns.
Spurious local sources due to long line and background noise.
Many spurious map sources due to field edge, long line, background noise.
```

```
Small window: Some spurious map sources due to background noise.


** EPIC PN

Full frame, large window and small window exposures.
Exposure durations of 18311, 3247 and 18100 seconds.

Full frame: Bright object off-centre with a bright out of time event.
Some other faint sources in the field. CCDs bright at end.
Single blank columns (missing data) in 5 CCDs.
All source lists affected by bright extended object.
Also spurious sources due to out of time event, CCD ends, background noise.

Large window: Bright object off-centre plus some other faint sources.
All source lists affected by bright extended object.
A few spurious local sources and spurious map sources due to background noise.

Small window: Bright object in one corner with out of time events.



** RGS1, RGS2

2 exposures from RGS1 and RGS2, durations of 45020 and 17010 seconds.
All CCDs working in RGS1.

Spectrum through middle of spatial extraction region.
Spectra within the spectral extraction regions on energy map.
Noisy spectrum in first order spectrum plot, very noisy spectrum in second.

2nd RGS1: All spectra are much fainter than in 1st RGS1.
No spectrum visible within second order spectral extraction region.
Very noisy spectra in the spectrum plots.

1st and 2nd RGS2: Spatial extraction region is central.
Otherwise as 1st and 2nd RGS1.


** OM

No products, listed as inactive in observation summary.
No ODF observation files.


** Catalogue cross-correlation products

Catalogue plot not fully in plot region at the edges.
A few XMM sources not already in the catalogue.
```

Fig.8 is composed of the images produced by PPS from the MOS1 and MOS2 Full and Partial windows respectively, while Fig. 9 shows the PPS images from the three PN exposures, in Full Frame, Small and Large Window modes respectively. All these products are considered fully acceptable.

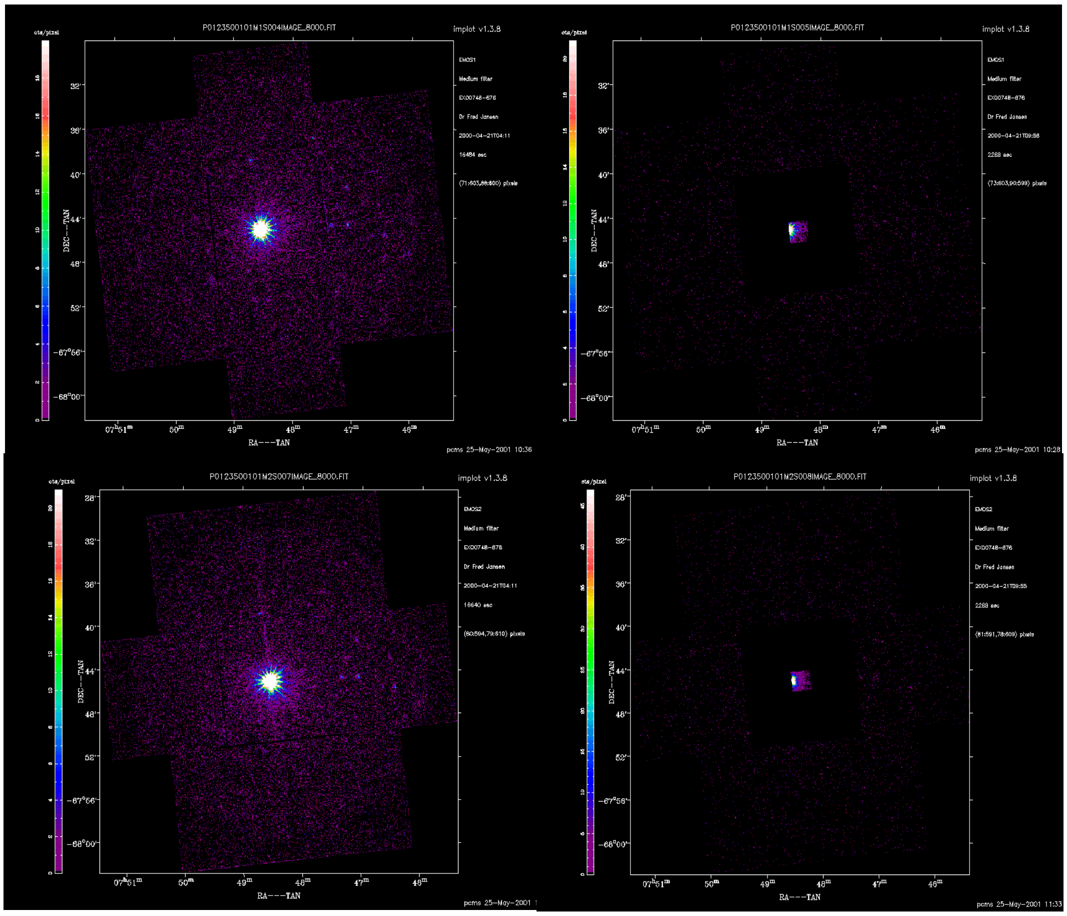

Figure 8: EXO 0748-676 EPIC MOS images: in the upper part the MOS1, in the lower part the MOS2 images in Full Window and Partial W2 window modes respectively

Fig. 10 shows the first and second order spectra derived by PPS from the first RGS1 exposure (45ksec).

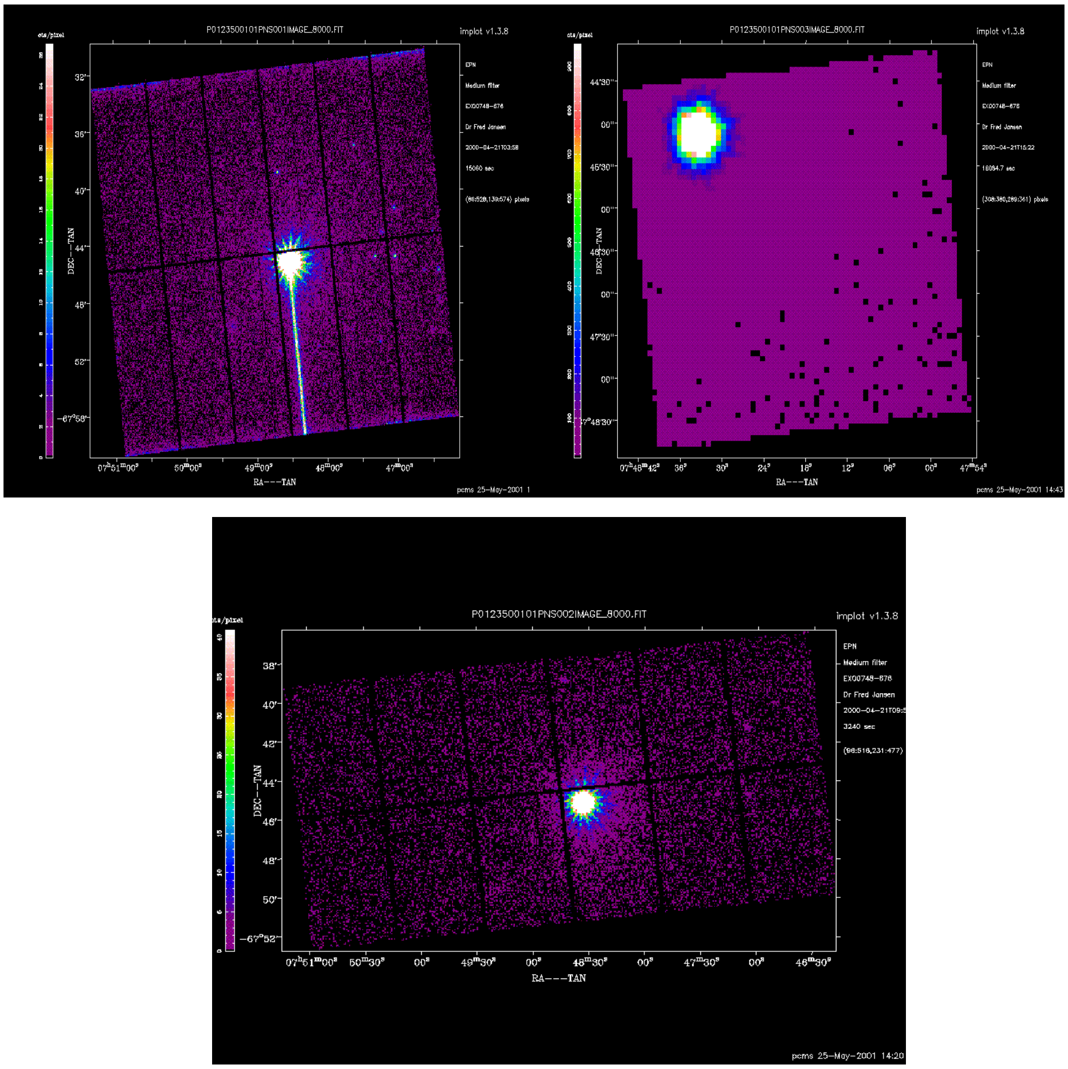

Figure 9: EXO 0748-676 EPIC PN images: in the upper part the Full Frame and Small window mode images, in the lower part the PN Large Window mode image.

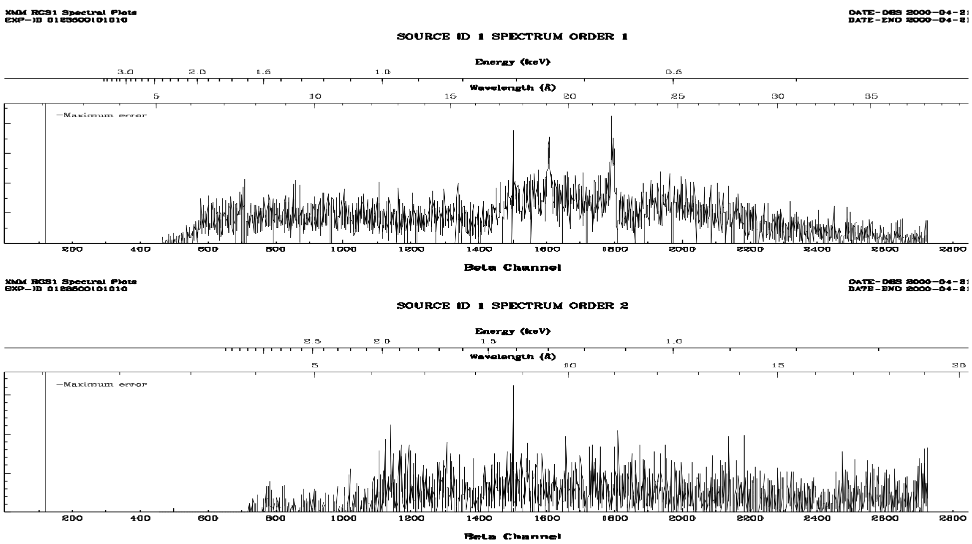

Figure 10: RGS1 first and second order spectra of EXO 0748-676

3.2.5 G21.5-09

XMM-Newton observed the region containing the Crab-like SuperNova Remnant (SNR) G21.5-09 ($\alpha_{2000} = 18^h33^m33^s.0$, $\delta_{2000} = -10°4534'10".0$) on April 7, 2000, between 12:35:28 and 22:57:20 UTC (revolution number 60). Warwick et al. (2001) have published preliminary scientific results of this observation.

```
XMM SSC data-product screening log
Version: <23-05-2001>

XMM  XMM                     PCMS
Rev  Obs Seq.    Target     Seq_id
060  0122700101  G21.5-09   000189


** GENERAL COMMENTS

No OM products, OM listed as inactive in observation summary.
No OM ODF observation files.


[EPIC comments refer, in general, to Energy-band 8.]

** EPIC MOS1

Full frame. Large bright central diffuse object plus a few other sources.
Faint noisy columns. All source lists affected by bright diffuse object.
Also spurious local sources due to background noise and a noisy column.
Many spurious map sources due to field edge, noisy columns, background noise.


** EPIC MOS2

Full frame. Large bright central diffuse object plus a few other sources.
Faint noisy columns. All source lists affected by bright diffuse object.
Also spurious local sources due to background noise.
Many spurious map sources due to field edge and background noise.


** EPIC PN

Full frame. Large bright diffuse object just off-centre. A few other sources.
Bright object produces a faint out of time events. CCDs bright at end.
Single blank columns (missing data) in 5 CCDs.
All source lists affected by bright diffuse object.
Also spurious local sources - out of time event, CCD ends, background noise.
Spurious map sources - out of time event, CCD ends, field edge, background.


** RGS1, RGS2
```

```
All CCDs working in RGS1.

No spectrum visible on spatial map.
Faint spectra within spectral extraction regions at one side on energy map.
Very noisy spectra in the spectrum plots.

RGS2: Spatial extraction region is central, otherwise as RGS1.


** OM

No products, listed as inactive in observation summary.
No ODF observation files.


** Catalogue cross-correlation products

Catalogue plot not fully in plot region at the edges.
A few XMM sources not already in the catalogue.
Some faint ROSAT sources not seen by XMM.
```

The PPS images of all three EPIC cameras are shown in Fig. 11. The verification of the accuracy of spectral fitting for, and of the cross-calibration among the EPIC cameras, is discussed in section 4.1. The PPS products are considered completely acceptable.

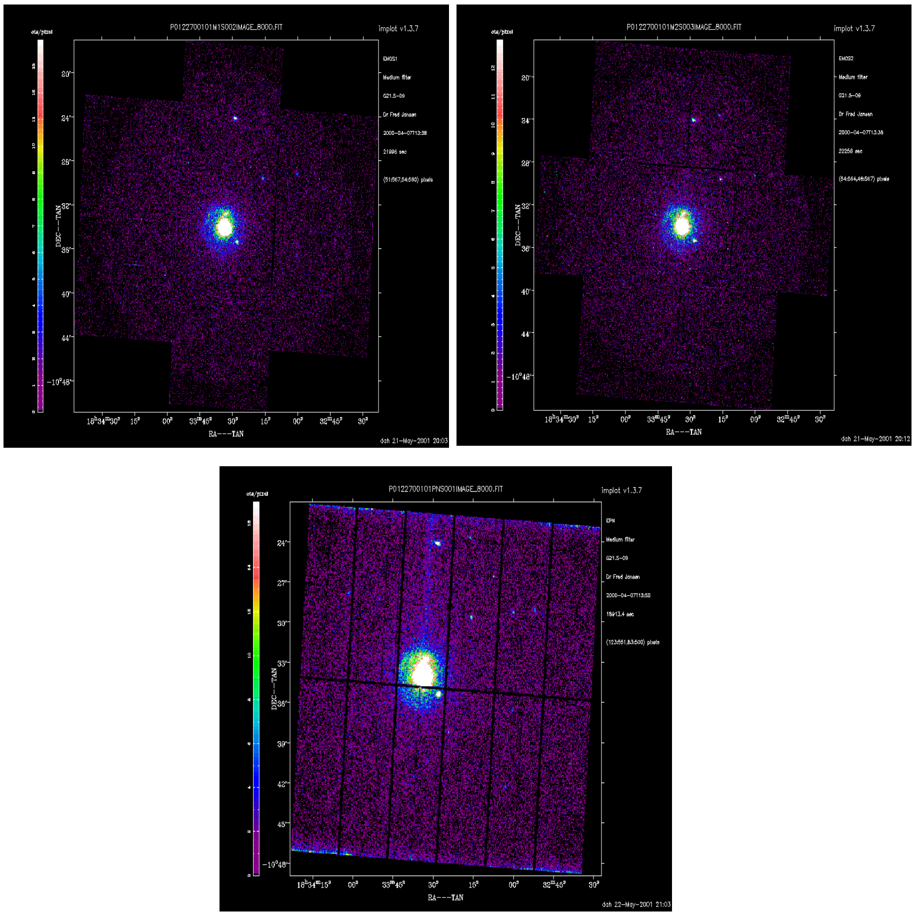

Figure 11: EPIC MOS1, MOS2 and PN images of G21.5-09

3.2.6 Lockman Hole:

The Lockman Hole field, centered on the sky position ($\alpha_{2000} = 10^h52^m43^s.0$, $\delta_{2000} = 57°28'48".0$), one of the most observed sky areas at all wavelengths, has been observed by XMM-Newton several times. We use for scientific validation purposes the almost 70 ksec observation performed in revolution 70, on April 27, 2000, between 02.46:15 UTC and 21:37:20 UTC.

```
XMM SSC data-product screening log
Version: <30-05-2001>

XMM  XMM                 PCMS
Rev  Obs Seq.   Target   Seq_id
070  0123700101 Lockman Hole  000209


** GENERAL COMMENTS

5 sets of OM exposures using 5 filters.
2 exposures from MOS1, RGS1 and RGS2.
2nd MOS1 exposure just shows a very bright background in the field of view.
MOS2 and PN had long exposure durations of 61290 and 62010 seconds.


[EPIC comments refer, in general, to Energy-band 8.]

** EPIC MOS1

2 full frame exposures (scheduled and unscheduled).
Exposure durations of 45999 and 14773 seconds.

Scheduled: A number of sources. Noisy columns.
Spurious local sources - noisy columns, CCD edges, field edge, background.
Also many spurious map sources.


** EPIC MOS2

No products.


** EPIC PN

Full frame. A number of sources. CCDs bright at end.
Single blank columns (missing data) in 5 CCDs.
Spurious local sources - diffuse areas, CCD ends, field edge and background.
Also many spurious map sources.


** RGS1, RGS2

2 exposures from RGS1 and RGS2, durations of 49020 and 18810 seconds.
```

```
All CCDs working in RGS1.

No spectra visible on spatial map and energy map.
Very noisy spectra in the spectrum plots.

2nd RGS1: Very bright background, otherwise as 1st RGS1.

1st and 2nd RGS2 as 1st and 2nd RGS1.


** OM

5 sets of exposures using the V, U, White, UVW1 and UVW2 filters.
Exposure durations of 1000, 1000, 1500, 2200 and 4400 seconds.
Only sets 1-4 have tracking plots.
Links to non-existent tracking plots in the OM summary.

V filter: Central ghost, loops (2 very bright) and faint long parallel lines.
Bright sources are over-exposed and a few have their own loops.
Some sources not detected in the source lists.
A few spurious sources due to bright loops and background noise.

U filter: Central ghost, loops (2 bright) and very faint long parallel lines.
Bright sources are over-exposed and a few have their own loops.
Some sources not detected in the source lists.
A few spurious sources due to bright loops and background noise.

White filter: Central ghost, loops (2 very bright), faint long parallel lines.
Diffuse region around the central ghost.
Bright sources show sharp diffraction patterns, a few have their own loops.
Some sources not detected in the source lists.
Some spurious sources due to loops, parallel lines and background noise.

UVW1 filter: Central ghost, loops (1 bright), very faint long parallel lines.
A few bright sources have their own faint loops.
Some sources not detected in the source lists.
A few spurious sources due to the ghost and loops.

UVW2 filter: A few sources not detected in the source lists.


** Catalogue cross-correlation products

Catalogue plot not fully in plot region at the corners.
Some XMM sources not already in the catalogue.
```

The most striking point concerning the products of this observation is the fact that the EPIC MOS2 event list is empty and so there are no products at all from this camera. The MOS2 camera was at a temperature below the one specified in the used calibration file (EMOS2_HKPARMINT_0005.CCF) as valid for pipeline processing. This CCF was unnecessarily restrictive and has been superseded by a new issue. Due to time and man power constraints pipeline re-processing has not taken place.

PPS products of EPIC MOS1 and PN are shown in Fig. 12. Despite of the problem with the MOS2 data the data set is considered acceptable.

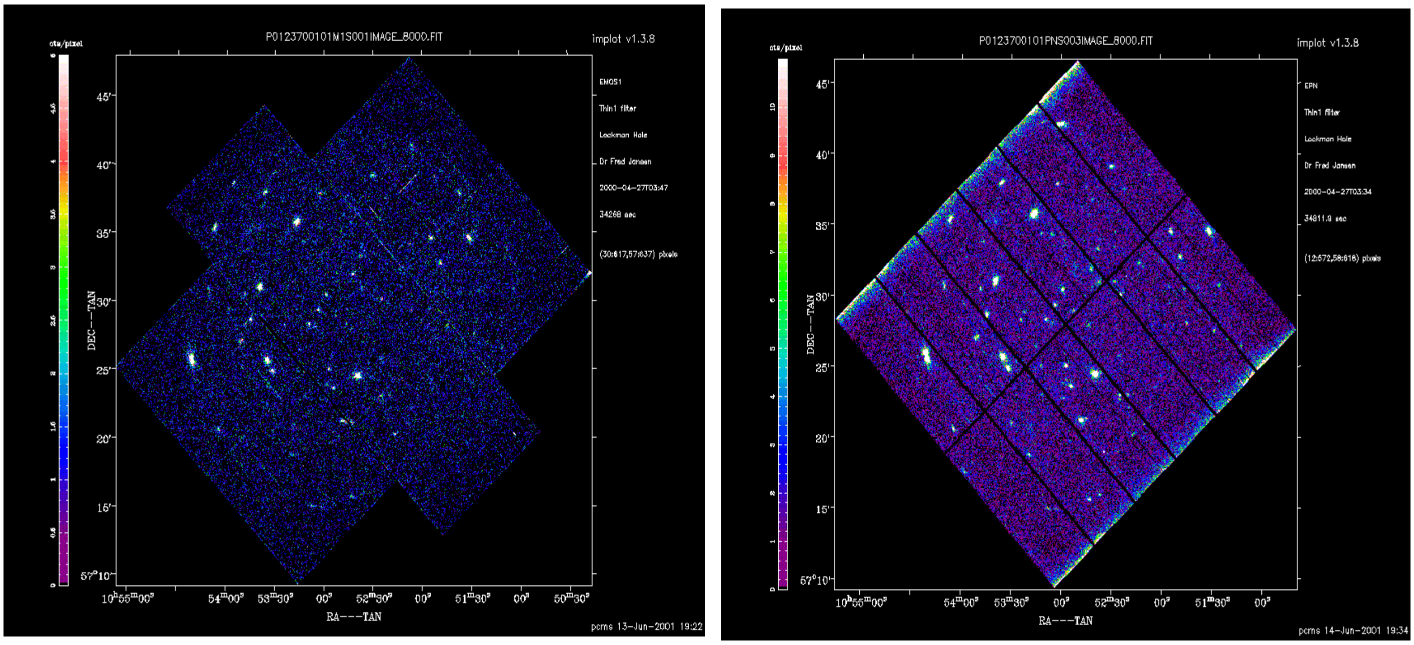

Figure 12: EPIC MOS1 and PN images of the Lockman Hole region

3.2.7 Markarian 421:

The BL Lac object Markarian 421, very bright at X-ray and UV wavelengths, is one of the RGS calibration targets. The observation used for this validation has been performed during CAL / PV phase, in revolution 84, with a total duration of 65 ksec.

```
XMM SSC data-product screening log
Version: <24-05-2001>

XMM  XMM                   PCMS
Rev  Obs Seq.    Target    Seq_id
084  0099280101  Mrk 421   000196


** GENERAL COMMENTS

No PN and OM products. PN in fast timing mode and OM filter invalid.
2 exposures from RGS1 and RGS2.
PN exposure is listed in PPS summary and EPIC summary.
MOS1 has shortest exposure duration, then MOS2, PN and 2nd RGS, then 1st RGS.


[EPIC comments refer, in general, to Energy-band 8.]

** EPIC MOS1

Timing mode. Very bright central object producing a bright line across field.
A few other sources in the field of view. Very faint noisy columns.
A few faint sources not detected in the local source list.
Spurious local sources due to the bright line and bright CCD inner edges.
Many spurious map sources due to bright line, CCD inner edges and field edge.


** EPIC MOS2

Small window. Very bright central object producing a bright line across field.
A few other sources in the field of view.
All source lists affected by bright extended object.
Spurious local sources due to bright line, CCD inner edges, background noise.
Many spurious map sources - bright line, CCD inner edges, field edge, noise.


** EPIC PN

No products, PN was in fast timing mode.


** RGS1, RGS2

2 exposures from RGS1 and RGS2, durations of 36500 and 27300 seconds.
All CCDs working in RGS1.
```

```
RGS1: Spatial extraction region off-centre on spatial map.
Very bright spectrum through middle of spatial extraction region.
Very bright spectra within the spectral extraction regions on energy map.
Also third and fourth order spectra visible on energy map.
Clear spectrum in first order spectrum plot, noisy spectrum in second plot.
2nd RGS1 as 1st RGS1.

RGS2: Spatial extraction region is central, otherwise as RGS1.
2nd RGS2 as 1st RGS2.


** OM

No products, filter was invalid.


** Catalogue cross-correlation products

Catalogue plot not fully in plot region at the edges.
A few faint XMM sources not already in the catalogue.
Some faint ROSAT sources not observed by XMM.
```

Fig. 13 shows the MOS2 image taken in Small Window free running (W4) mode, with the well centered source. Figs. 14 and 15 are the spatial and order images, and the resulting spectra corresponding to the RGS1 first exposure, lasting for almost 37 ksec.

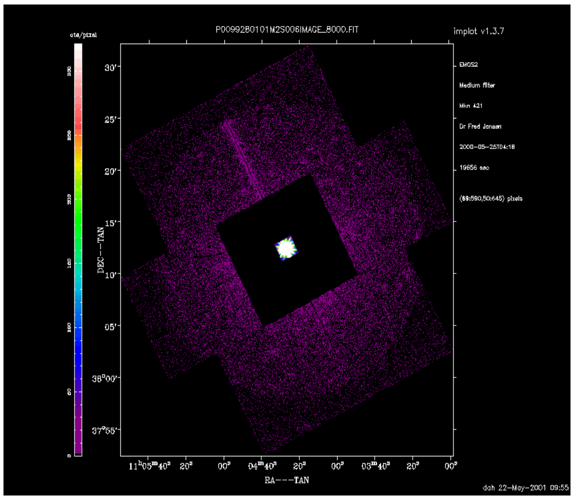

Figure 13: EPIC MOS2 image of Markarian 421, taken in small window free running mode

The results of the interactive analysis based on the PPS output of Mrk421 are contained in section 4.2, in which both the MOS and the RGS data are showing serious deficiencies.

3.2.8 PKS 0558-504

The bright quasar PKS 0558 - 504 observation ($\alpha_{2000} = 05^h59^m47^s.0$, $\delta_{2000} = -50°26'51".0$) we use for validation has been performed in revolution 153. It was used for final commissioning of

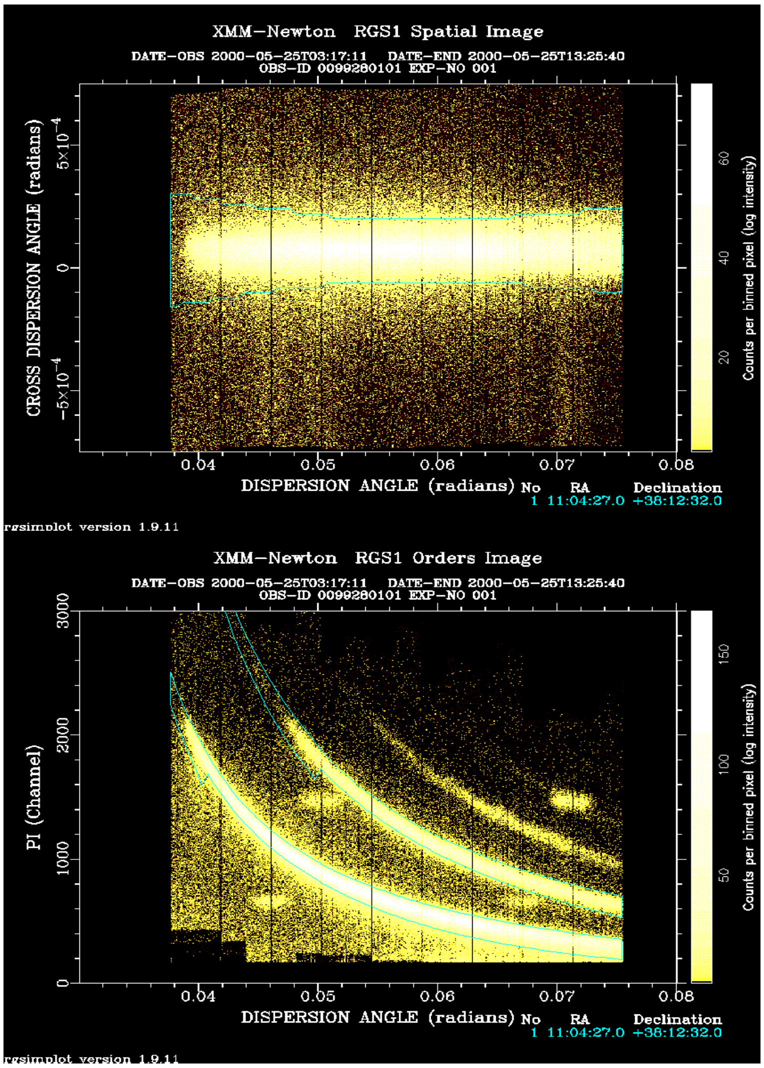

Figure 14: Markarian 421 RGS1 spatial and orders image

the OM Fast Mode.

```
XMM SSC data-product screening log
Version: <23-05-2001>

XMM  XMM                    PCMS
Rev  Obs Seq.    Target     Seq_id
153  0129360201  PKS0558-504 (FAST te)  000188


** GENERAL COMMENTS

2 exposures from MOS1, MOS2 and PN. Only have 4 OM central exposures.
No OM products from a further set of exposures taken with Magnifier over OM.
MOS and PN have shorter exposure durations than RGS.


[EPIC comments refer, in general, to Energy-band 8.]
```

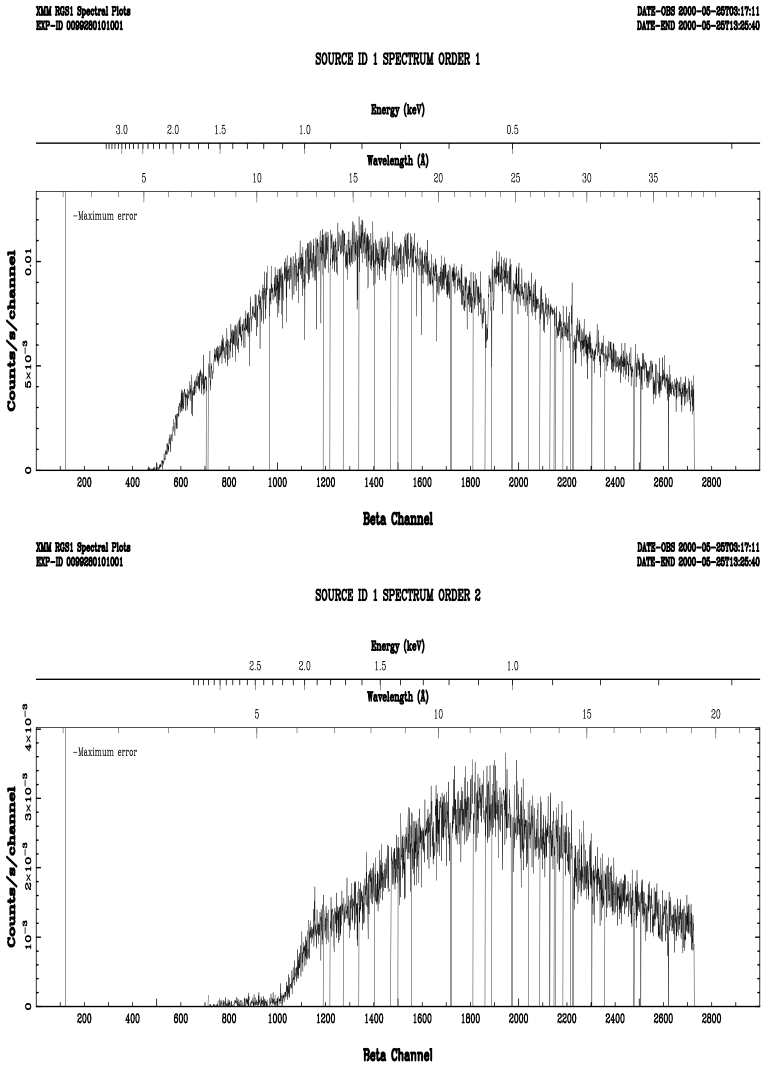

Figure 15: Markarian 421 first and second order spectra

```
** EPIC MOS1

Large window and full frame exposures, durations of 7900 and 12800 seconds.
Bright central object with large cross of faint line through middle of field.
Some other sources in the field of view. Very faint noisy columns.
All source lists affected by bright extended object.
Also a few spurious local sources due to background noise.
Many spurious map sources due to field edge and background noise.


** EPIC MOS2

As MOS1.


** EPIC PN

Small window and full frame exposures, durations of 10700 and 8600 seconds.
```

```
Bright object just off-centre producing a bright out of time events.
Some other sources in the field of view. CCDs bright at the ends.
Single blank columns (missing data) in a few CCDs.
All source lists affected by bright extended object.
Also spurious local sources due to out of time events.
Spurious map sources due to out of time event, field edge, background noise.


** RGS1, RGS2

Bright spectrum through middle of spatial extraction region.
Bright spectrum within first order spectral extraction region on energy map.
Fainter spectrum within second order spectral extraction region.
Noisy spectrum in first order spectrum plot, very noisy spectrum in second.
RGS2 as RGS1.


** OM

Only have 4 central exposures using the UVW1 filter.
Exposure durations of 1200 seconds.
Faint central ghost and faint long parallel lines visible.
Bright sources are over-exposed.
Some sources not detected in the source lists.


** Catalogue cross-correlation products

Catalogue plot not fully in plot region at the corners.
A few XMM sources not already in the catalogue.
```

Fig. 16 shows the MOS1 images taken in Full Window and Partial W3 modes (MOS2 exposures were taken in parallel in the same configuration) above, and the PN images in Full Frame and Small window modes. The EPIC data set is considered acceptable. A deeper analysis of these products follows in the next section.

Concerning OM, there are no products from the exposures with Magnifier, since this mode is not yet commissioned (and therefore not supported by the SAS). OM fast mode is also not yet supported by SAS.

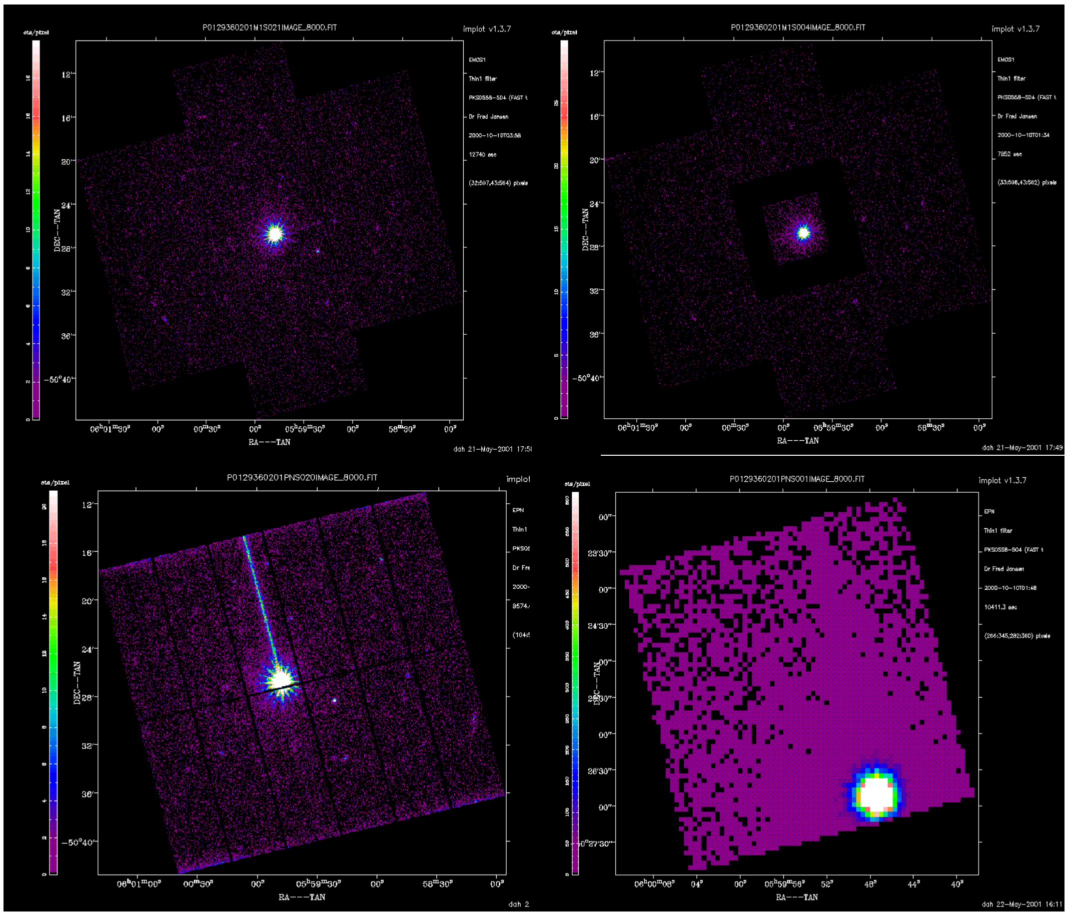

Figure 16: EPIC MOS1 and PN images of PKS 0558 - 504

4 Interactive Analysis results

Despite of future work based on all these processed reference data (there is still work going on, which cannot be included anymore in the report), we have so far limited the analysis to a couple of fundamental questions:

- EPIC spectral fitting
- RGS spectral response matrices
- RGS wavelength accuracies

4.1 Quality of EPIC spectral fitting

Response matrices for EPIC spectral fitting can be obtained with SAS v5.1 in three ways:

1. generating a redistribution matrix via the SAS task `rmfgen` and an effective area vector via the SAS task `arfgen`
2. generating an effective area vector via the SAS task `arfgen`, using a standard redistribution matrix (available through the web page `http://xmm.vilspa.esa.es/ccf`) as input to `arfgen` to calculate consistently the energy grids
3. using a standard response matrix file, again available through the web page `http://xmm.vilspa.esa.es/ccf`

We remind that a "response file" (extension `*.rsp`) is a ready-made combination of a redistribution matrix (extension `*.rmf`) and an ancillary file vector (extension `*.arf`). For more details we advise the reader to look at the HEASARC OGIP memos, such as
`http://heasarc.gsfc.nasa.gov/docs/heasarc/caldb/docs/memos/cal_gen_92_002/cal_gen_92_002.html`.

All the above outlined methods are available and fully functional for all EPIC cameras with SAS v.5.1. A comparison of their performances has been carried out using the observations of the Crab-like SuperNova Remnant (SNR) G21.5-0.9 (Warwick et al. 2001), and of the quasar

Scenario	Γ	N_H (10^{22} cm^{-2})	χ^2/ dof
MOS1			
1.	$1.92\pm^{0.02}_{0.03}$	2.36 ± 0.04	285.8/183
2.	$1.95\pm^{0.03}_{0.02}$	2.40 ± 0.04	240.0/183
3. (`PATTERN=0-12`)	$1.86\pm^{0.02}_{0.03}$	2.28 ± 0.04	222.2/183
3. (`PATTERN=0`)	$1.90\pm^{0.04}_{0.03}$	$2.32\pm^{0.06}_{0.04}$	184.5/172
MOS2			
1.	$1.86\pm^{0.03}_{0.02}$	2.28 ± 0.04	332.0/183
2.	1.90 ± 0.03	2.29 ± 0.04	211.9/183
3. (`PATTERN=0-12`)	1.82 ± 0.03	2.19 ± 0.04	235.6/183
3. (`PATTERN=0`)	1.86 ± 0.03	$2.22\pm^{0.05}_{0.04}$	211.8/170
p-n			
1.	1.93 ± 0.02	$2.36\pm^{0.04}_{0.03}$	422.0/224
2.	1.96 ± 0.02	$2.42\pm^{0.03}_{0.04}$	353.0/224
3. (`PATTERN=0`)	1.86 ± 0.02	2.24 ± 0.03	324.1/224
3. (`PATTERN=0-4`)	1.87 ± 0.02	$2.28\pm^{0.02}_{0.03}$	290.4/212

Table 2: G21.5-0.9 observation best-fit parameters. Errors are at the 90% confidence level for one interesting parameter. Indices refer to the three "paths" available to generate EPIC response matrices with SAS v5.1

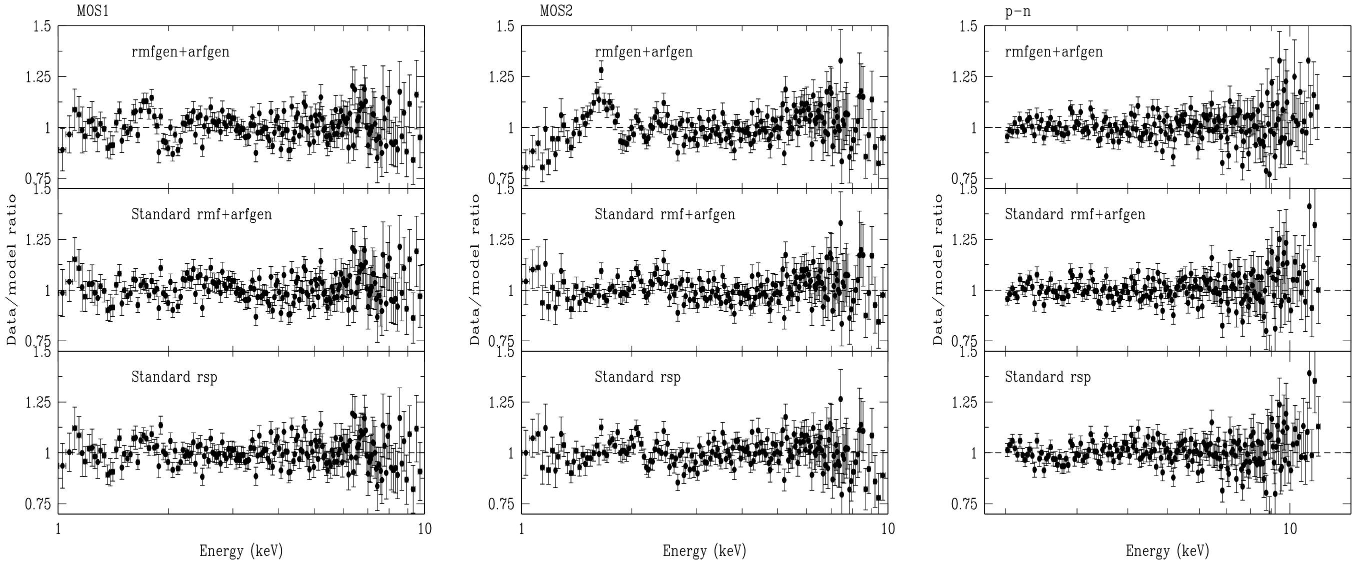

Figure 17: Data/model ratio when a photoelectrically absorbed power-law model is applied to the G21.5-0.9 spectra of MOS1 (*left panel*), MOS2 (*central panel*) and p-n (*right panel*). From *top* to *bottom*: matrices wholly generated with SAS v5.1; standard redistribution matrix plus SAS-generated effective area; standard response files. The fit parameter values used for the figures are given in Tab. 2.

PKS0558-504 (O'Brian et al. 2001). The former spectrum is well described by a strongly absorbed ($N_H \sim 2\times10^{22}$ cm^{-2}) power-law. It is therefore particularly well-suited to compare the performances of the response matrices above 1 keV. The latter is a quasar with a prominent soft excess. It will be therefore mainly used in the following to compare the response performances in the soft X-ray regime.

The standard response matrix files used in this report are:

- `m[12]_${filter}v9q19t5r5_${pattern}_15.rsp` for the MOS cameras, where `${filter}` is either `thin1` or `med` and `${pattern}` is either `all` or `p0`
- `epn_ff20_s[ d]Y9_${filter}.rmf` for the p-n camera, where `${filter}` is either `thin` or `medium` (the extensions of these files are admittedly non compliant with the OGIP convention)

The standard redistribution matrices used in this report are:

- `m[12]_r5_${pattern}_15.rmf` for the MOS cameras
- `epn_ff20_s[ d]Y9.rmf` for the p-n camera

In the following, uncertainties are quoted at the 90% confidence level for one interesting parameter, and each data point corresponds to a signal-to-noise ratio >3.

A comparison of the EPIC response matrix performances, together with some practical suggestions about how to use them, is given also by Saxton & Siddiqui (2001)

4.1.1 G21.5-09

The EPIC cameras were all operating during this observation in Full Frame mode. The source was on-axis. Source spectra have been extracted from circular regions of 1' radius around the centroid of the SNR. Background spectra have been extracted from an annulus of 3.15' to 4.6' radius. The source spectra have been rebinned in order to have at least 50 counts in each spectral bin and to oversample the instrumental energy resolution by a factor not higher than 3. A detector map has been extracted for each EPIC camera and used as an input to `arfgen`, since the centroid of the nebula is surrounded by an extended halo. The spectra have been fit in the 1-10 keV and 1-12 keV energy bands for MOS and p-n, respectively. The model employed is a simple power-law with photoelectric absorption.

The residuals (expressed in terms of data/model ratio), are generally within ±5% (the scatter is largely dominated by statistical uncertainties below this level). As shown in Fig. 17, residuals at the level of ±10% are present in the MOS spectra between 1.8 and 2.5 keV even if the standard redistribution matrices are used. They are mostly due to uncertainties in the modeling of the optics gold edges. The residuals in this energy band increase at the 20% level in the MOS2 if wholly SAS-generated matrices are employed. Residuals of this amount are larger than typically observed with XMM-Newton (cf. Fig. 20 and Saxton & Siddiqui 2001), and are likely to be due to the coupling between the systematic uncertainties in the response matrix and the strong photoelectric cut-off in G21.5-09. They are likely to be therefore mainly representative of the behavior of strongly absorbed sources. In the p-n, an excess emission below 1.5 keV is also present (not shown in Fig. 17 for clarity; cf. Warwick et al. 2001 and Fig. 19).

The MOS1 residuals exhibit an excess emission around the energy of the iron K_α fluorescent line. If standard response matrices are used, this feature can be formally parameterized with a Gaussian profile ($\Delta\chi^2 = 7.8$ for a decrease by 2 in the number of degrees of freedom, corresponding to a 95.0% confidence level). The best fit parameters are: centroid energy, $E = 6.80\pm^{0.08}_{0.32}$ keV, intrinsic width $\sigma = 0.2 \pm 0.2$ keV and equivalent width $EW = 40\pm^{40}_{20}$ eV. The same feature is, however, not present either in the MOS2 ($EW < 40$ eV) or in the p-n ($EW < 11$ eV) residuals.

Spectral indices yielded by the fit with wholly or partly SAS-generated matrices tend to be slightly steeper than those obtained with the standard response files. The difference is $\Delta\Gamma \simeq 0.06$ and $\Delta\Gamma \simeq 0.09$ for scenarios 1. and 2. above, respectively. Given the strong correlation between the spectral index and the photoelectric absorption column density, this reflects in a $\Delta N_H \simeq 0.8$–1.2×10^{21} cm^{-2}.

In Fig. 18 we compare the spectral fitting results in the three EPIC cameras, with respect to the two quantities that uniquely identify the employed model. The best-fit values are generally in agreement within the statistical uncertainties.

If one sets `modelee=yes` in `arfgen`, the fluxes measured via spectral fitting in scenarios 1. and 2. above are encircled-energy corrected, and can be therefore directly compared. This is done in Tab. 3. The fluxes agree within about 1–2%. It is interesting to notice that the p-n

Scenario	MOS 1	MOS 2	p-n
1.	5.04 ± 0.02	5.07 ± 0.02	4.724 ± 0.015
2.	5.02 ± 0.02	5.02 ± 0.02	4.645 ± 0.014

Table 3: Observed 2–10 keV flux in scenarios 1. and 2., when `arfgen` is run with `modelee=yes` (*i.e.*: encircled-energy correction activated)

measurements are systematically ≃6% lower than the MOS ones. Such difference is not observed in the analysis of a point-like source (cf. Tab. 4). This may be related to the extended nature of G21.5-09, implying a still not fully correct treatment of the correction when a detector map is used. Users interested in analysis of extended sources are urged to employ the usual grain of salt when evaluating the absolute flux measurements obtained with the SAS v5.1 response matrices.

The standard response matrix files are generated under the assumption of infinite extraction

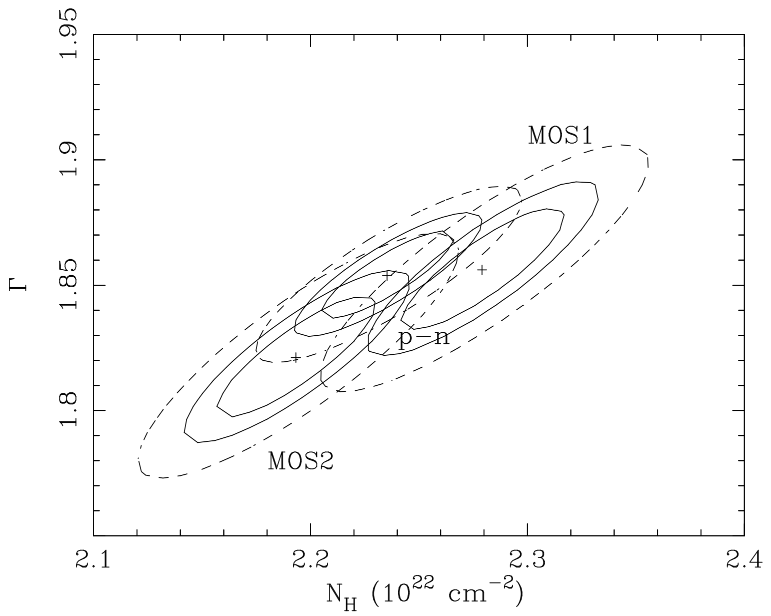

Figure 18: N_H versus Γ iso-χ^2 contour plots for the EPIC spectra of G21.5-0.9. Contours are at the 68%, 90% (*solid lines*) and 99% (*dashed lines*) confidence level for two interesting parameters. Standard response matrices are used.

region, and the fluxes obtained with them must be therefore corrected *a posteriori* for the aperture flux losses. We remind, moreover, that the encircle energy correction is properly applied in SAS v5.1 only if the extraction region has a circular shape. This point is discussed in details by Saxton & Siddiqui (2001).

4.1.2 Effect of the pattern selection

The SAS task `rmfgen` can currently cope only with standard choices of the pattern selection: `PATTERN=0-12` and `PATTERN=0` for the MOS and p-n, respectively. However, standard response matrices are available also for MOS `PATTERN=0` and p-n `PATTERN=0-4` (*i.e.*: single and double events). The best-fit parameters (cf. Tab. 2) and the quality of the spectral fits (cf. Fig. 19) are not substantially dependent on the pattern selection choice.

4.1.3 PKS0558-504

In the observation of PKS0558-504 two exposures were taken with each of the EPIC cameras, in Full Frame and in a windowed mode, respectively. The former are likely to be affected by pile-up, and we will not deal with them in this report. The results reported below refer therefore to the exposures taken in Large Window and Small Window modes for MOS and p-n, respectively. The source was on-axis. Spectra have been extracted from circular areas of radius of 1'.5 (MOS) and 2' (p-n). Standard grade selections have been adopted: `PATTERN=0-12` and `PATTERN=0` for the MOS and p-n, respectively. Background spectra have been extracted from source-free nearby areas on the same chip where the centroid of PKS0558-504 lays. For sources of such a brightness level (4.65 ± 0.02 s^{-1} and 16.20 ± 0.06 s^{-1} in the MOS 1 and p-n, respectively), the background contributes to less than 10% in each spectral bin below 10 keV under "quiet" radiation background environments. Response matrices have been generated with `arfgen` and `rmfgen`, with `modelee=yes` and default flat detector maps.

The spectra have been fit with a model constituted by a power-law and two blackbodies (*baseline*

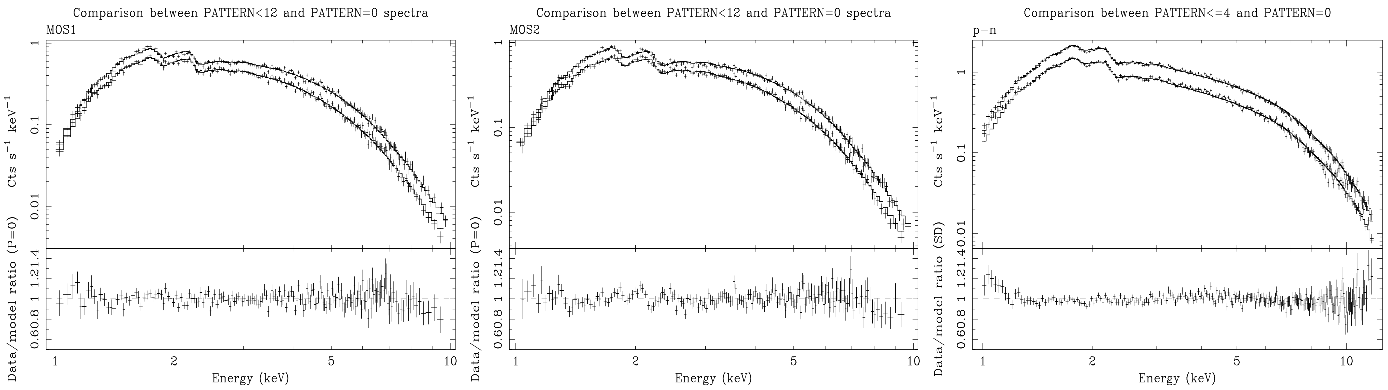

Figure 19: Comparison between the MOS spectra obtained with `PATTERN=0` and `PATTERN=0-12` (*left* and *central* panel) and between the p-n spectra with `PATTERN=0` and `PATTERN=0-4` (*right* panel). In all plots the *lower* panel shows the residuals against a photoelectrically absorbed power-law for the "non-standard" pattern selection only (*i.e.*: `PATTERN=0` for MOS and `PATTERN=0-4` for p-n)

model; the third blackbody envisaged by O'Brian et al. 2001 is actually not required by the fit of this dataset). The power-law component dominates above 2 keV, the blackbodies account for the bulk of the prominent soft X-ray excess. The best-fit parameters and results are summarized in Tab. 4. In Fig. 20 the residuals against the best-fit model are shown, when the model is

Instrument	Γ	kT^1_{BB} (eV)	N^1_{BB} (10^{-5})	kT^2_{BB} (eV)	N^2_{BB} (10^{-3})	F (0.1-2 keV) (10^{-11} erg cm^{-2} s^{-1})	F (2–10 keV)	χ^2/ dof
MOS 1	$2.17\pm^{0.04}_{0.02}$	162 ± 7	$5.6\pm^{1.3}_{0.6}$	$33.3\pm^{1.7}_{1.0}$	3.4 ± 0.7	1.10	2.32	175.7/128
MOS 2	2.12 ± 0.07	$169\pm^{12}_{13}$	$5.8\pm^{1.7}_{0.9}$	36 ± 2	$2.0\pm^{0.5}_{0.4}$	1.23	2.27	120.4/102
p-n	2.15 ± 0.06	$139\pm^{9}_{8}$	12.0 ± 1.3	$56\pm^{4}_{3}$	$0.35\pm^{0.04}_{0.03}$	1.10	2.32	151.0/140

Table 4: PKS0558-504 best-fit parameters. kT and N are the temperature and the normalization of the blackbody components. F is the measured flux

separately applied to the spectra of the three cameras. Focusing mainly on the energy bandpass below 2 keV (above this energy the scatter in the residuals is largely dominated by the statistical uncertainties), the relative residuals are well within a ±5% in the p-n and ±10% in the MOS cameras. However, significant differences are present between the MOS and the p-n. This is illustrated in Fig. 21, where the results of a *simultaneous* fit of all spectra with the same model and all the model parameters (except the normalizations) tied together is shown. In the range 0.3–2 keV the p-n spectrum is significantly steeper than the MOS ones. This trend is reversed below 0.3 keV, where the MOS spectra exhibit a prominent (and probably spurious; cf. Grandi et al., in preparation) soft excess and the p-n residuals drop (cf. Fig. 3 in Saxton & Siddiqui 2001). Similar results are reported by La Palombara & Molendi (2001) with different combinations of instrumental modes.

The measured fluxes agree within a 2–3%, except in the MOS 2 soft (*i.e.* 0.1–2 keV) energy bandpass, where the flux is discrepant by about 10% (cf. Tab. 4).

4.1.4 Mrk 421

Mrk 421 was observed with MOS2 in Partial Window free running readout mode (W4). This mode has been used so far in several observations but it is not going to be a mode of choice of AO2 because of the difficulties for calibration. However, we have performed spectral fitting,

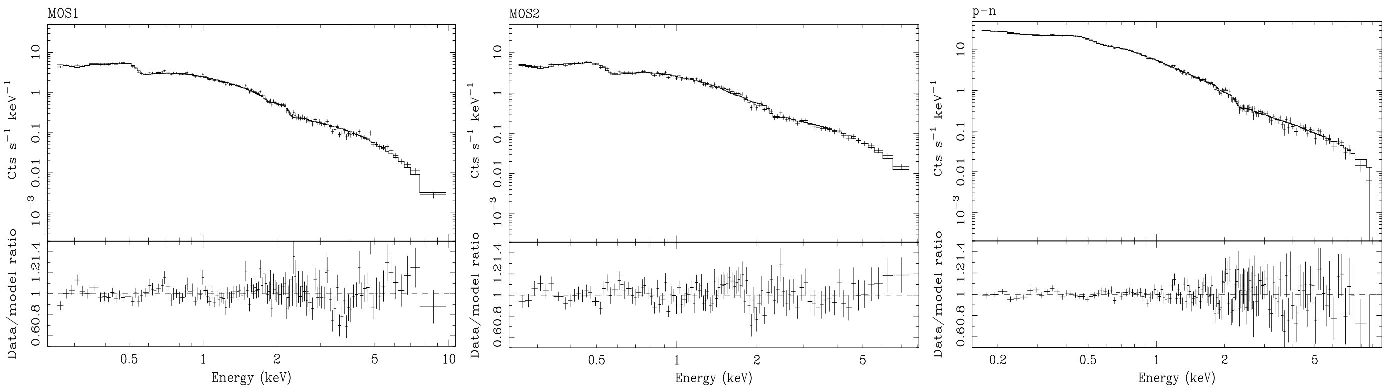

Figure 20: PKS-558-504 spectra (*upper panels*) and residuals in units of data/model ratio (*lower panels*) when the baseline model is *separately* applied to the spectra of MOS 1 (*left*), MOS 2 (*center*) and p-n (*left*).

mainly motivated by the need of simultaneous fitting with RGS data (see section 4.2).

It has been shown already by Brinkmann et al (2001) using MOS and PN data that the spectrum of Mrk 421 can be well approximated at first order with a broken power-law model. Figure 22 shows clearly the problems caused in this mode up to 1.5 keV by the lack of on-board voltage linearization ("Gatti" correction). It causes an artificial oscillation in the spectrum. However, the qualitative description of the spectrum by the model is acceptable, and above 1.5 keV rather good.

4.1.5 Future improvements

Improvements in this field are rapid and continuous. At the time this report was compiled, new calibration files and response matrices were being delivered, which significantly improve the quality of the spectral fitting in some of the areas outlined above, in particular with respect to:

- MOS residuals between 1.8 and 2.5 keV
- p-n soft response

The users are urged to consult regularly the XMM-Newton calibration page (`http://xmm.vilspa.esa.es/calibration/`). One may also consider subscribing the `sas-ccf` mailing list. Regular updates on the status of the XMM-Newton payload calibration are regularly sent.

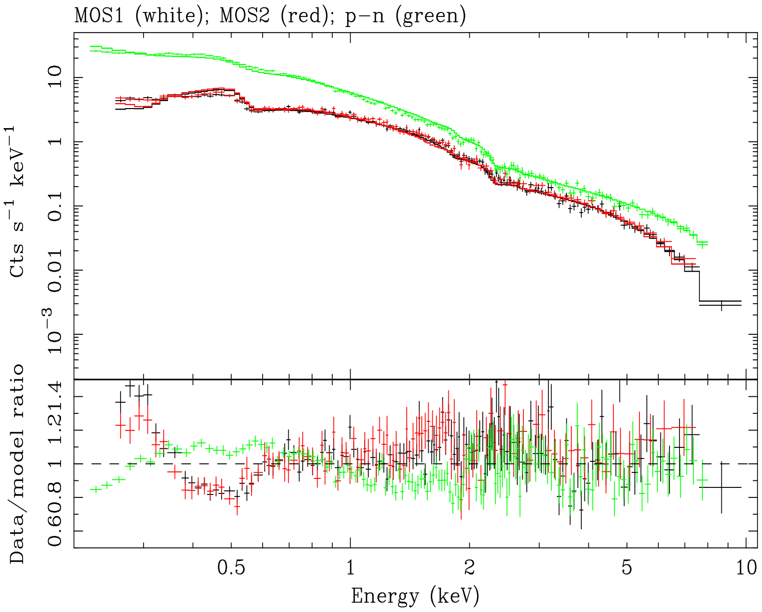

Figure 21: PKS0558-504 spectra (*upper panel*) and residuals in units of data/model ratio (*lower panel*) when the same baseline model is applied simultaneously to the spectra of all the EPIC cameras: MOS 1 (*black*), MOS 2 (*red*) and p-n (*green*)

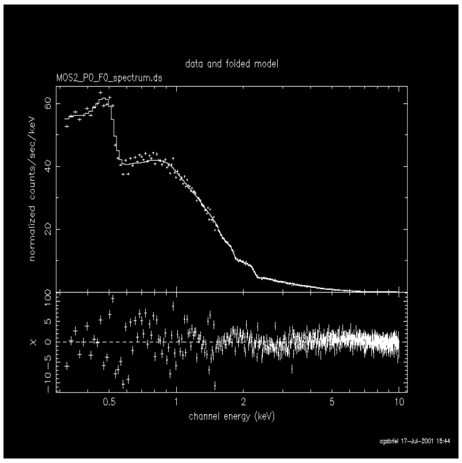

Figure 22: EPIC MOS2 data and model fit of Mrk 421

4.2 RGS effective area

Generation of the response matrix for the RGS instruments is performed by the SAS task rgsrmfgen. There are so far no standard matrices for RGS, since they depend very much on the position of the source in the FOV. A bug in the task rgsrmfgen was discovered soon after public release of SAS 5.1, which should be affecting the high energy part of the effective area determination, in a way that is very dependent on the spatial and energy cuts applied to the data. In the following we quote the XMM-News #6 from July 23:

"A serious coding error has been detected in the RGS response matrix generator task included in the recently released SAS version 5.1. The effect of this error is to return effective area values above 1 keV which deviate substantially from the correct values. A software fix has been identified; however, due to the dependency of this software package on other components in the SAS, there cannot be an isolated release of a fixed version of this particular package. The XMM-Newton Science Operations Centre, together with the RGS team, is working on a full new release of the SAS in the near future. Given the availability of people over the summer holidays, this new release is expected early September 2001.

In the mean time the only practical workarounds is to ignore the data above 1 keV. Rolling back to SAS 5.0 is, for this particular RGS data analysis problem, also a possibility."

A further problem related to the backwards incompatibility is also addressed in the same issue, namely:

"An unrelated, but equally painful error is related to RGS specific PPS products (like e.g. the RGS calibrated event list produced by the PPS), created in the PPS before June 18, 2001 (i.e. created with PPS versions earlier than 02000035/20010618.143655 2001-06-18T14:36:55). Tasks in version 5.1.0 of the SAS cannot be used to extract spectra and generate response files for the affected event lists. The affected tasks are: rgsspectrum, rgsrmfgen, rgsfluxer. The problem is caused by a file format change. This error will be corrected by the time of the above mentioned new SAS release."

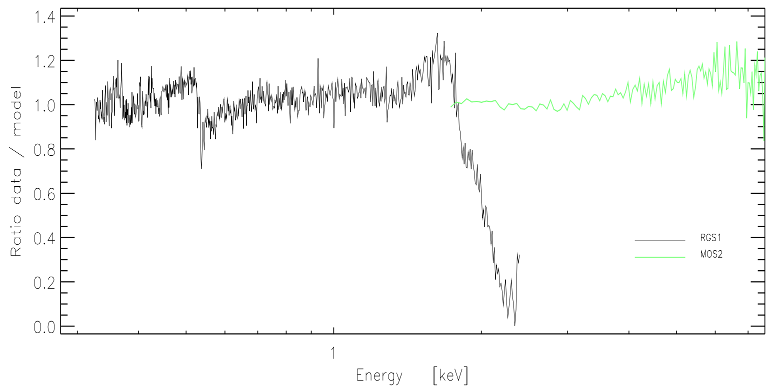

Figure 23: Mrk 421: RGS1 and MOS2 data / model ratio from simultaneous fitting

We have used the Mrk 421 data for assessing qualitatively the effect of the wrong effective area returned by rgsrmfgen. As shown in 4.1.4 the spectrum can be approximated using a broken power law model. We have fitted simultaneously the RGS1 spectrum and the high energy part of the MOS spectrum. The resulting data / model ratios both for RGS1 and MOS2 (Fig. 23) show clearly the deficiencies above 1.4 keV, as well as around the K-shell photoelectric threshold energy of O_I (at $E = 0.55$ keV; Erd 2000). The fit results, although not too meaningful, are close to the values achieved in the SAS 5.0 validation report of Mrk 421 (Ehle et al, 2001): $\Gamma_1 = 1.863 \pm 0.005$, $\Gamma_2 = 2.205 \pm 0.002$, $E_{break} = 0.842 \pm 0.07$.

In order to see the differences between RGS1 and RGS2 we have approximated the first order spectra simultaneously with the same model, leaving the normalization free between the two sets. Fig. 24 shows that the relative differences between RGS1 and RGS2 are for the entire spectrum well below 10%.

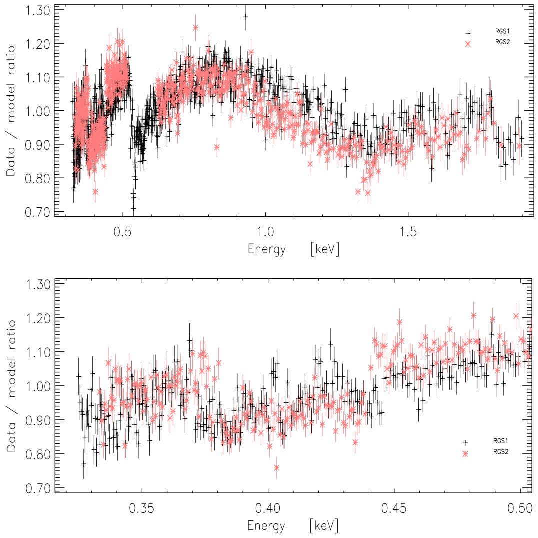

Figure 24: Mrk 421: RGS1 and RGS2 data / model ratio from simultaneous fitting

4.3 RGS wavelength accuracy

In order to assess the wavelength accuracy we have analyzed the data corresponding to the AB Doradus and Capella observations. It was necessary to reprocess the Capella data, because the coordinates originally entered in the proposal were wrong. The specification of a wrong pointing direction yields misplaced selection regions and inaccurate wavelength scale. After computing the effective areas using rgsrmfgen, XSPEC was used for obtaining the spectra from the pipeline products. It is not expected that deviations in the effective areas affect the wavelength accuracy of the RGS observations. The AB Doradus first and second order spectra of RGS1 and RGS2 are shown in Fig. 25.

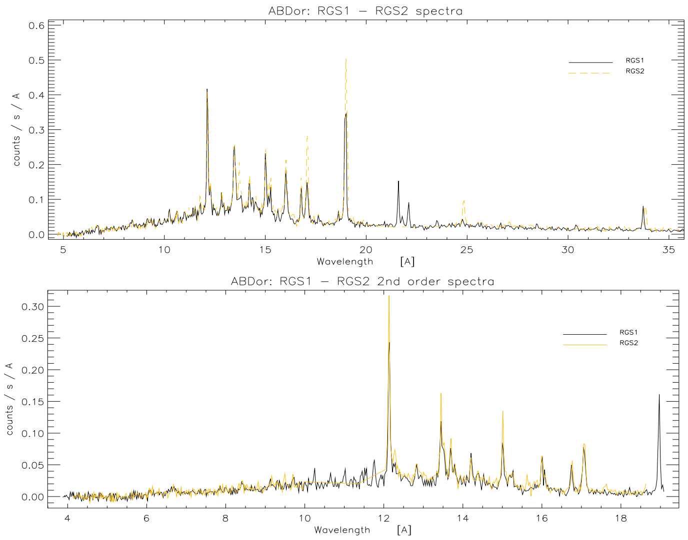

Figure 25: AB Dor: RGS1 and RGS2 first and second order spectra

In a first attempt we have approximated the data with the vmekal model using XSPEC. Figure 26 shows a detail of the results obtained with the second order spectrum.

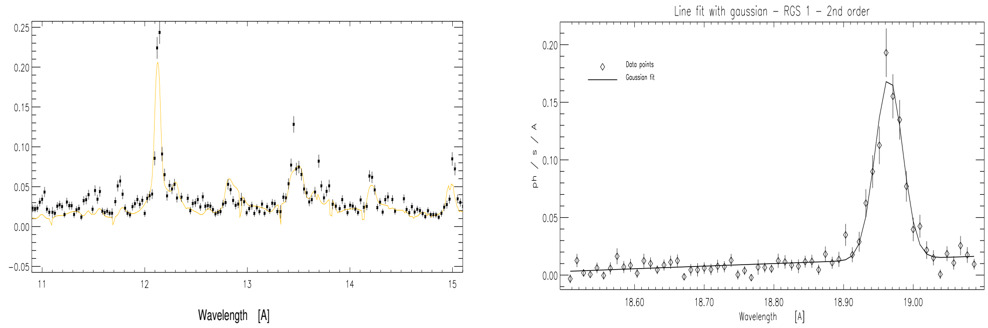

Figure 26: *Left panel*:AB Dor: RGS1 2nd order spectrum detail with vmekal fit - *Right panel*: Fitting a spectral line with a gaussian

For establishing the wavelength accuracies we have fitted the data with the sum of a gaussian and a quadratic term in the regions of intense line emission, using the IDL function GAUSSFIT. For the purposes of establishing the position of the main spectral lines this is sufficient in most of the cases, although in some cases due to the non-resolution of multiplets the result is not accurate. Visual inspection is therefore necessary. Figure 26, right panel, is an example of plotting the approximation with gaussian plus quadratic term over the points for confirming visually the quality of the wavelength determination.

Table 5: Spectral lines found in AB Dor - RGS1 and RGS2 - first and second order spectrum

Transition	λ_{lab}	RGS1 λ	RGS1 **Width**	RGS1 Δ	RGS2 λ	RGS2 **Width**	RGS2 Δ
Ne X Ly_alpha	12.134 *	12.1336	0.026	0.000	12.1355	0.028	0.002
Ne IX He_alpha	13.448 P	13.4549	0.030	0.007	13.4484	0.030	0.000
Fe XVII(27 - 1)	15.014 *	15.0133	0.028	0.001	15.0128	0.030	-0.001
Fe XVIII	16.006 P	*16.0190*	*0.046*	*0.013*	*16.0343*	*0.048*	*0.041*
Fe XVII(5 - 1)	16.780 *	16.7742	0.026	-0.006	16.7740	0.030	-0.006
Fe XVII(3 - 1)	17.055 P	*17.0633*	*0.035*	*0.008*	*17.0712*	*0.040*	*0.016*
O VIII Ly_alpha	18.969 *	18.9690	0.036	0.000	18.9706	0.029	0.002
O VII He_alpha (1st)	21.602 *	21.5925	0.028	-0.009			
N VII Ly_alpha	24.781 *	*24.7568*	*0.034*	*-0.024*	24.7754	0.039	-0.006
C VI Ly_alpha	33.736 *	33.7231	0.034	-0.013	33.7287	0.034	-0.007

The lines in italics are examples of discarded lines by visual inspection. The large widths of the gaussian are due to not resolved multiplets. The Fe XVII(3 - 1) is actually a doublet at 17.053 17.100 A, both components of approximately same intensity. The N VII Ly_alpha is right between two CCDs by RGS1 and therefore the center is ill determined. If we take just the reliable lines:
RGS1: $\bar{\Delta} = (-2.9 \pm 6.3)mA \quad (|\bar{\Delta}| = 4.6mA)$
RGS2: $\bar{\Delta} = (1.4 \pm 4.1)mA \quad (|\bar{\Delta}| = 2.6mA)$

Transition	λ_{lab}	RGS1 λ	RGS1 **Width**	RGS1 Δ	RGS2 λ	RGS2 **Width**	RGS2 Δ
Ne X Ly_alpha	12.134 *	12.1342	0.019	0.000	12.1332	0.019	-0.001
Ne IX He_alpha	13.448 P	13.4511	0.028	0.003	13.4524	0.015	0.004
Fe XVII(27 - 1)	15.014 *	15.0080	0.018	-0.006	15.0122	0.018	-0.002
Fe XVIII	16.006 P	16.0004	0.015	-0.006	16.0048	0.020	-0.001
Fe XVII(5 - 1)	16.780 *	16.7742	0.026	-0.006	16.7740	0.030	-0.006
Fe XVII(3 - 1)	17.055 P	*17.0648*	*0.035*	*0.010*	*17.0727*	*0.032*	*0.022*
O VIII Ly_alpha	18.969 *	18.9651	0.019	-0.004			

Taking the reliable lines:
RGS1: $\bar{\Delta} = (-3.1 \pm 3.5)mA \quad (|\bar{\Delta}| = 4.2mA)$
RGS2: $\bar{\Delta} = (-1.2 \pm 3.2)mA \quad (|\bar{\Delta}| = 2.8mA)$

*) RGS-COL-CAL-00-007
P) Phillips et al, A&A Suppl. Ser. 138, 381

Several spectral lines, as found by the procedure, have been compared with literature values. Tables 5 and 6 summarize the results. The Capella observation we have analyzed has been used as one of the wavelengths calibrators, therefore it does not constitute an independent set. The results of the AB Dor data analysis show a high accuracy in the wavelength calibration with mean deviations from the literature values of few mA and a variance of less than 7 mA. No single line was significantly outside the nominal accuracy of 8 mA as quoted by the RGS instrument team.

Table 6: Spectral lines found in Capella - RGS1 and RGS2 - first and second order spectrum

		RGS1			RGS2		
Transition	λ_{lab}	λ	**Width**	Δ	λ	**Width**	Δ
Si XIII Ly_alpha	6.648	6.644	0.019	-0.004	6.659	0.033	0.011
Ne X Ly_alpha	12.134 *	12.133	0.022	-0.001	12.137	0.022	0.003
Ne IX He_alpha	13.448 P						
Fe XVII(27 - 1)	15.014 *	15.021	0.029	0.007	15.023	0.033	0.009
Fe XVIII	16.006 P						
Fe XVII(5 - 1)	16.780 *	16.780	0.027	0.000	16.779	0.028	-0.001
Fe XVII(3 - 1)	17.055 P						
O VIII Ly_alpha	18.969 *	18.973	0.029	0.004	18.976	0.031	0.007
O VII He_alpha (1st)	21.602 *	21.606	0.027	0.004			
N VII Ly_alpha	24.781 *	*24.769*	*0.040*	*-0.012*	24.784	0.033	0.003
C VI Ly_alpha	33.736 *	33.733	0.029	-0.003	33.740	0.037	0.004

Taking the reliable lines:

RGS1: $\bar{\Delta} = (1.0 \pm 3.8)mA \quad (|\bar{\Delta}| = 3.3mA)$

RGS2: $\bar{\Delta} = (1.4 \pm 2.6)mA \quad (|\bar{\Delta}| = 2.6mA)$

		RGS1			RGS2		
Transition	λ_{lab}	λ	**Width**	Δ	λ	**Width**	Δ
Si XIII Ly_alpha	6.648	6.655	0.012	0.007	6.657	0.005	0.009
Ne X Ly_alpha	12.134 *	12.134	0.014	0.000	12.133	0.016	-0.001
Ne IX He_alpha	13.448 P	13.452	0.017	0.004	13.454	0.017	0.006
Fe XVII(27 - 1)	15.014 *	15.013	0.017	-0.001	15.014	0.020	0.000
Fe XVIII	16.006 P	16.006	0.015	0.000	16.007	0.017	0.001
Fe XVII(5 - 1)	16.780 *	16.776	0.017	-0.004	16.779	0.017	-0.001
Fe XVII(3 - 1)	17.055 P	*17.066*	*0.036*	*0.011*	*17.056*	*0.021*	*0.001*
O VIII Ly_alpha	18.969 *	18.970	0.018	0.001			

Taking the reliable lines:

RGS1: $\bar{\Delta} = (1.0 \pm 3.3)mA \quad (|\bar{\Delta}| = |2.4|mA)$

RGS2: $\bar{\Delta} = (2.3 \pm 3.8)mA \quad (|\bar{\Delta}| = |3.0|mA)$

*) RGS-COL-CAL-00-007

P) Phillips et al, A&A Suppl. Ser. 138, 381

Appendix A: list of calibration files used by arfgen, rmfgen and rgsrmfgen

The following calibration files have been used in this report to produce effective area vectors with arfgen and rgsrmfgen:

- EMOS[12]_FILTERTRANSX_0009.CCF
- EMOS[12]_LINCOORD_0015.CCF
- EMOS[12]_MODEPARAM_0006.CCF
- EMOS[12]_PATTERNLIB_0005.CCF
- EMOS[12]_QUANTUMEF_0006.CCF
- EPN_PATTERNLIB_0001.CCF
- EPN_QUANTUMEF_0008.CCF
- RGS[12]_CROSSPSF_0002.CCF
- RGS[12]_LINCOORD_0007.CCF
- RGS[12]_LINESPREADFUNC_0003.CCF
- RGS[12]_QUANTUMEF_0006.CCF
- RGS[12]_REDIST_0004.CCF
- XMM_ABSCOEFS_0004.CCF
- XMM_BORESIGHT_0015.CCF
- XMM_MISCDATA_0011.CCF for arfgen
- XMM_MISCDATA_0013.CCF for rgsrmfgen
- XRT[2]_XAREAEF_0008.CCF
- XRT[13]_XAREAEF_0007.CCF
- XRT[23]_XENCIREN_0002.CCF
- XRT[12]_XPSF_0004.CCF
- XRT[3]_XPSF_0002.CCF

The following calibration files have been used to generate the redistribution matrix with rmfgen:

- EMOS[12]_PATTERNLIB_0005.CCF
- EMOS[12]_QUANTUMEF_0006.CCF
- EMOS[12]_REDIST_0007.CCF
- EPN_REDIST_0005.CCF
- XMM_ABSCOEFS_0004.CCF
- XMM_MISCDATA_0011.CCF

Acknowledgment

The authors acknowledge a careful reading and useful comments from C.Erd, J.W.den Herder and R.Saxton.

References

Audard M., et al (2001), A&A, 365, L329

Brinkmann et al (2001), A&A, 365, L162

Bonnet-Bidaut et al (2001), A&A, 365, L282

Cottam J., et al (2001), A&A, 365, L277

Ehle et al (2001), XMM-SOC-USR-TN-0003, available at
`ftp://xmm.vilspa.esa.es/pub/odf/data/sv/0099280101/0099280101_report.pdf.gz`

Gabriel C., Guainazzi M., Altieri B., XMM-SAX-VILSPA/2000-105/Dc Draft 0.5 (2000)

Güdel M., et al (2001), A&A, 365, L336

La Palombara N.,. Molendi S., 2001, Minutes of the EPIC Calibration Meeting, Leicester 6-7 June 2001

O'Brian P., et al, 2001, A&A, 365, L122

R.Saxton & H.Siddiqui, 2001, XMM-SOC-PS-TN-43, Version 2.0, available at
`ftp://xmm.vilspa.esa.es/pub/ccf/doc/rmfgen_report_21.ps.gz`

Warwick R.S, et al, 2001, A&A, 365, L248